Arbovirus-vector protein interactomics identifies Loquacious as a co-factor for dengue virus replication in *Aedes* mosquitoes

Short title: Loquacious is a dengue virus co-factor in mosquitoes

Benoit Besson[1], *Oscar M. Lezcano*[1], *Gijs J. Overheul*[1], *Kirsten Janssen*[1], *Cornelia G. Spruijt*[2], *Michiel Vermeulen*[2], *Jieqiong Qu*[1], *Ronald P. van Rij*[1]

[1]Department of Medical Microbiology, Radboud Institute for Molecular Life Sciences, Radboud University Medical Center, P.O. Box 9101, 6500 HB Nijmegen, the Netherlands

[2]Department of Molecular Biology, Faculty of Science, Radboud Institute for Molecular Life Sciences, Oncode Institute, Radboud University Nijmegen, 6525 GA Nijmegen, the Netherlands

Corresponding author: ronald.vanrij@radboudumc.nl

ABSTRACT

Efficient virus replication in *Aedes* vector mosquitoes is essential for the transmission of arboviral diseases such as dengue virus (DENV) in human populations. Like in vertebrates, virus-host protein-protein interactions are essential for viral replication and immune evasion in the mosquito vector. Here, 79 mosquito host proteins interacting with DENV non-structural proteins NS1 and NS5 were identified by label-free mass spectrometry, followed by a functional screening. We confirmed interactions with host factors previously observed in mammals, such as the oligosaccharyltransferase complex, and we identified protein-protein interactions that seem to be specific for mosquitoes. Among the interactors, the double-stranded RNA (dsRNA) binding protein Loquacious (Loqs), an RNA interference (RNAi) cofactor, was found to be essential for efficient replication of DENV and Zika virus (ZIKV) in mosquito cells. Loqs did not affect viral RNA stability or translation of a DENV replicon and its proviral activity was independent of its RNAi regulatory activity. Interestingly, Loqs colocalized with DENV dsRNA in viral replication organelles in infected cells and directly interacted with high affinity with DENV RNA in the 3' untranslated region *in vitro* (K_D = 100-200 nM). Our study provides an interactome for DENV NS1 and NS5 and identifies Loqs as a key proviral host factor in mosquitoes. We propose that DENV hijacks a factor of the RNAi mechanism for replication of its own RNA.

AUTHOR SUMMARY

Dengue virus is a mosquito-transmitted virus endemic to the tropics and subtropics, affecting an estimated 390 million people yearly. While the mechanisms of infection, pathogenesis and immune evasion have been extensively studied in humans, replication in *Aedes* mosquitoes has received much less attention, despite being a critical step in the arbovirus transmission cycle. Here,

39 we used a proteomic approach to identify *Aedes* mosquito proteins recruited by dengue virus non-
40 structural proteins NS1 and NS5. In addition to previously established host proteins that interact
41 with DENV in mammals, we identified Loquacious, a double-stranded RNA binding protein
42 involved in the antiviral RNAi immune response of mosquitoes. Unexpectedly, our data showed
43 Loquacious functions as a proviral factor that is recruited to replication organelles to facilitate viral
44 RNA replication. We propose that DENV exploits host immune components, such as Loquacious,
45 for its own benefit.
46

INTRODUCTION

Mosquito-borne flaviviruses such as dengue virus (DENV) and Zika virus (ZIKV) are transmitted between humans by *Aedes* mosquitoes, causing major public health and economic burden in the tropics and subtropics [1]. Whereas *Aedes aegypti* is considered the most common vector for DENV transmission, vector competence of *Ae. albopictus* and its ability to adapt to colder climates raise concerns of a shift of arbovirus endemic regions toward the Northern hemisphere, further enhanced by global warming [2–5]. As no specific treatment against DENV is available and vaccine development faces many obstacles [6], there is a need to understand the mechanisms of flavivirus replication in mosquitoes to developed transmission blocking strategies.

Flaviviruses have a single-stranded positive-sense RNA genome, which is translated upon release into the host cell and replicated at the membrane of the endoplasmic reticulum (ER) where viral proteins hijack the host cell machinery to form membrane invaginations functioning as viral replication organelles [7]. While structural proteins are essential for viral entry, assembly and release of viral particles, non-structural (NS) proteins together with host factors are required for viral RNA replication and modulation of host cell functions. Expressed in the lumen of the ER and released outside of the host cell, NS1 is an important pathogenicity factor in mammals [8,9]. In addition, NS1 contributes to the formation of viral replication organelles and recruits the oligosaccharyltransferase (OST) complex, as well as mRNA translation and protein folding factors [10–12]. As the viral RNA-dependent RNA polymerase, NS5 cooperates with other viral and host proteins to replicate the viral RNA, but also interacts with host proteins to suppress Jak-STAT signaling and modulate the spliceosome [13].

For transmission to a mammalian host, arboviruses need to efficiently replicate in their mosquito vector, which, like in mammals, requires extensive virus-host protein-protein interactions. Flavivirus host factors have been extensively studied in mammalian models using proteomics [10,13–15] as well as other high-throughput approaches such as RNAi and CRISPR screens [11,16–19]. In comparison, few studies have addressed host factors in mosquitoes. While it is likely that flaviviruses use homologous host proteins and cellular processes in mosquitoes and mammals, this has only been confirmed for few proteins, such as SEC61 [14,19]. In addition, given the evolutionary distance, the different physiologies and diverse immune systems of mosquitoes and mammals, it is to be expected that flavivirus proteins additionally interact with specific sets of proteins in mosquito vector and vertebrate host.

A key element differentiating mosquito and mammalian immunity is the crucial role of RNAi in antiviral defense in insects [20–22]. Double-stranded (ds)RNA formed during viral replication is cleaved by the nuclease Dicer-2 into small interfering (si)RNA duplexes that are loaded into Argonaute 2 (Ago2) to guide the recognition and cleavage of complementary viral RNA. Loading of siRNA duplexes into Argonaute proteins is facilitated by the paralogous dsRNA-binding proteins R2D2, Loquacious (Loqs) and Loqs2, the latter of which is unique to *Aedes* mosquitoes [23–27]. The *Ae. aegypti Loqs* gene encodes multiple, non-redundant spice isoforms [24], of which Loqs-PB along with R2D2 facilitates siRNA processing, whereas Loqs-PA is required for microRNA (miRNA) processing [24]. In line with a function in siRNA processing, it was found that silencing *R2D2*, *Dicer-2* and *Ago2* increased DENV replication [28]. In addition, the mosquito specific Loqs2 interacts with Loqs and R2D2 and is essential to control systemic flavivirus infections *in vivo* [23]. Note that *Loqs* transcript annotation of the reference genome AaegL5 does not correspond to the annotation used in [24]. The transcript referred to as *Loqs-RA* by Haac et al.

92 [24] corresponds to *Loqs-RB* in AaegL5 and *vice versa*. The transcript referred to as *Loqs-RC* by
93 Haac et al. does not exist in AaegL5. In the current manuscript, we use the AaegL5 annotation.
94
95 To identify host proteins interacting with DENV proteins in mosquitoes, we purified FLAG-tagged
96 DENV NS1 and NS5 expressed in the context of all DENV non-structural proteins, followed by
97 quantitative mass spectrometry. We identified Loqs as an essential co-factor for DENV and ZIKV
98 RNA replication, independent of its function in RNAi. We showed that Loqs interacts with the 3'
99 untranslated region of DENV RNA and localizes to viral replication organelles during infection of
100 *Aedes* cells. Our data provide new insights into flavivirus replication in mosquitoes and illustrate
101 a case in which a potential antiviral protein, Loqs, is recruited by a virus for its own benefit.
102

RESULTS

Interactome of DENV NS1 and NS5 proteins in *Aedes* mosquito cells

To identify host factors that interact with DENV proteins in an RNA-independent manner in mosquitoes, we established a system to express all non-structural proteins in *Ae. albopictus* cells. Expression of non-structural proteins in the absence of viral RNA is sufficient to induce membrane rearrangements, reminiscent of those induced during viral infections [7,29]. All non-structural genes were cloned under the control of an *Ae. aegypti* poly-ubiquitin promoter (PUb), introducing a 3xFLAG tag at the N-terminus of NS1 after the ER localization signal and conserving the signal peptidase cleavage site, or at the C-terminus of NS5, according to previous work [10,13] (Fig. 1A). Expression of the recombinant proteins was confirmed by western blot, and both FLAG-tagged NS1 and NS5 were efficiently concentrated by FLAG-immunoprecipitation (Fig. 1B). As expected, NS1 and NS5 were expressed in distinct cell compartments in *Ae. albopictus* C6/36 cells (Fig. 1C).

Using a plasmid expressing untagged DENV non-structural proteins as a control, we characterized the interactome of FLAG-tagged NS1 and NS5 in C6/36 cells by label-free mass spectrometry (Fig. 1D-E and Table S1). NS1 interacted with 55 proteins, including the viral NS2A, NS3, NS4A and NS4B proteins, whereas NS5 interacted with 45 proteins, including NS1, NS2A, NS3 and NS4A, and a total of 15 host proteins interacted with both NS1 and NS5 (Fig. 1D-E, 2A and Table S1). NS2B peptides were not detected, likely due to limitations of detection. However, given that NS2B is a cofactor for the NS3 protease and polyprotein processing was efficient (Fig. 1B), NS2B is likely expressed at physiologically relevant levels in our system. The identification of viral non-structural proteins in NS1 and NS5 immunoprecipitations confirmed the formation of

125 macromolecular complexes in the absence of structural proteins and viral RNA in our experimental
126 system.
127 Biological processes and functional protein network analysis identified several functional protein
128 clusters in association with NS1 and NS5 (Fig. 2B-C). Among the cellular interactors enriched at
129 least two-fold in NS1 immunoprecipitations, we identified 11 proteasome subunits and five
130 proteins of the OST complex (Fig. 1D-E, 2 and Table S1): Oligosaccharide transferase Δ subunit
131 (OstΔ, ortholog of human ribophorin II, RPN2), Oligosaccharide transferase γ subunit (OSTγ,
132 ortholog of human MAGT1), UDP-glucose-glycoprotein glucosyltransferase (UGGT, ortholog of
133 human RPN1), Oligosaccharyltransferase 48kD subunit (OST48, ortholog of human dolichyl-
134 diphosphooligosaccharide-protein glycosyltransferase non-catalytic subunit, DDOST) and
135 catalytic subunit 3A of the oligosaccharyltransferase complex (STT3B). Amongst the cellular
136 interactors enriched in NS5 immunoprecipitations, we identified three elements of the survival of
137 motor neuron (SMN) complex involved in the spliceosome and small nuclear ribonucleoprotein
138 (snRNP) assembly (Gemini 2, Gemini 3 and Smn) as well as the E3 ligase HYD (ortholog of
139 human UBR5). The OST complex and proteasome have previously been described as proviral host
140 factors interacting with DENV NS1 in mammals [10,30–32], NS5 was shown to hijack the snRNP
141 and human ortholog UBR5 was purified with NS5 in mammals [13], illustrating virus-host
142 interactions that occur both in the mosquito vector and human host. Together, these data validate
143 our experimental model to identify physiologically relevant protein-protein interactions between
144 virus and vector.
145
146 **Identification of DENV proviral and antiviral host factors**

From the 79 host proteins interacting with NS1 and/or NS5, we selected 22 hits for a functional knockdown screen in the RNAi competent *Ae. albopictus* U4.4 cell line (Fig. 3A). Cells were transfected with dsRNA, infected with DENV, and viral RNA was quantified by RT-qPCR. From the initial screen (Fig. 3B), 10 hits were selected for a confirmation screen with a second set of dsRNA, targeting a different region of the gene to avoid off-target effect (Fig. 3C). We classified genes as high or low-confidence hits, based on selective criteria for gene knockdown efficiency, effect on gene knockdown on DENV RNA levels, and consistency between both dsRNA data sets. One NS1 interactor was identified as proviral factor as silencing consistently resulted in a decrease in viral RNA (Fig. 3B-C), Loquacious (Loqs, ortholog of human TARBP2) as well as two NS5 interactors: the E3 ubiquitin-protein ligase HYD (ortholog of human UBR5) and Muskelin. In addition, four NS1 interactors were found to be antiviral as silencing consistently resulted in an increase in viral RNA (Fig. 3B-C): OSTΔ (RPN2), RNA polymerase I subunit H or RPL12 (ortholog of human RPA12), DISCO-interacting protein 1 (DIP1, ortholog of human ADARs), ER retention protein RER1 in addition to one common NS1/NS5 interactor: HSP60A.

Among the hits, the RNAi cofactor *Loqs* had the strongest phenotype with up to 70-90% inhibition of DENV RNA levels upon its knockdown (Fig. 3B-C). Two potential Loqs host interactors were also included in the functional screen (Fig. 2). *Pancreatic eIF2A-α kinase* (*PEK*), distant ortholog of human PRKRA known to interact with the human *Loqs* ortholog TARBP2, of was not efficiently silenced, and knockdown of RNA helicase *Gemini 3* (ortholog of human DEAD box helicases like DDX20) [33–36] did not modulate DENV replication (Fig. 3C). The finding that Loqs was a proviral host factor is unexpected, given that Loqs is an essential cofactor of RNAi, a pathway with antiviral activity in mosquitoes. For this reason and because of the strong NS1 association (Fig. 1D-E) and consistent phenotype (Fig. 3B-C), we focused the remainder of the

study on Loqs, using *Ae. aegypti* as a model, for which a better genome annotation is available than for *Ae. albopictus*.

Loqs is a flavivirus proviral factor in *Ae. aegypti*

The *Loqs* gene encodes three splice isoforms, which differ from each other by the presence or absence of short exons. Loqs-RA and Loqs-RB are very similar to each other, except that the 144 nt-long exon 5 is retained in Loqs-RA. Loqs-RC is a shorter isoform, in which exon 6 is retained, but exon 7 is skipped (Fig. 4A). As a consequence, the gene products Loqs-PA and Loqs-PB contain two dsRNA-binding domains (dsRBD, IPR014720) as well as a Staufen, C terminal domain (IPR032478), which may be involved in protein-protein interactions. Loqs-PC contains only the two N-terminal dsRBDs.

From the mass spectrometry data, we identified one peptide unique to Loqs-PA in NS1 immunoprecipitations, whereas other peptides were shared between the three isoforms. Using primers flanking exon5 (Fig. 4C, Table S3) as well as unique primers to distinguish the isoforms (Fig. 4D, Table S3), we showed that Loqs-RA and Loqs-RB are expressed at similar levels in *Ae. aegypti* Aag2 cells, whereas Loqs-RC is only lowly expressed, in line with its low expression *in vivo* (Fig. S1A). Together, these results indicate that NS1 interacts with Loqs-PA, although we cannot rule out interactions with Loqs-PB and Loqs-PC (Fig. 4B).

To analyze which of the isoforms is responsible for the observed proviral phenotype, we compared DENV replication after RNAi-mediated knockdown of specific *Loqs* isoforms as well as other components of the miRNA and siRNA pathways in Aag2 cells (Fig. 4E). Silencing of *Ago2* resulted in an increase in viral replication, in agreement with an antiviral function of the RNAi pathway, whereas *R2D2* and *Loqs2* silencing did not significantly affect DENV replication in cells.

193 *Ago1* silencing was also associated with an increase in viral replication, suggesting an important
194 function of miRNA regulated genes in viral replication. In contrast, silencing of all *Loqs* isoforms
195 combined resulted in a 60% reduction in DENV RNA levels (Fig. 4E), confirming our
196 observations *Ae. albopictus* U4.4 cells (Fig. 4B-C). Furthermore, silencing of the Loqs-RA isoform
197 specifically was associated with a 43% reduction in DENV replication, whereas Loqs-RC silencing
198 did not affect DENV replication, in line its low expression (Fig. 4E). Due to the *Loqs* gene
199 structure, it was impossible to design dsRNA that specifically targets Loqs-RB but not the other
200 isoforms. These results indicate that Loqs-PA and perhaps Loqs-PB are proviral host factors for
201 DENV replication in *Ae. aegypti*.
202 To further characterize the role of Loqs in flavivirus replication, we compared the effect of *Loqs*
203 silencing on DENV and ZIKV replication over time. *Loqs* silencing reduced viral RNA levels for
204 both viruses at all time points analyzed (Fig. 4F). Furthermore, the effect of *Loqs* silencing on viral
205 replication was consistently stronger for ZIKV (up to 90% inhibition at 48 h). In contrast and as
206 expected, *Ago2* silencing resulted in an increase in DENV and ZIKV RNA levels (Fig. 4F). These
207 results suggest that Loqs is a pan-flavivirus proviral host factor in *Aedes* mosquitoes.
208
209 **Loquacious proviral activity is independent of its RNAi regulatory functions**
210 Having established the importance of Loqs for flavivirus replication, we further characterized its
211 role during viral replication. To analyze the effect of Loqs on viral RNA stability and translation,
212 we monitored the expression of *Renilla* luciferase from a DENV subgenomic replicon in cells in
213 which *Loqs* was silenced [37]. To this end, luciferase expression was monitored after transfection
214 of replicon RNA into *Ae. albopictus* U4.4 cells and *Ae. aegypti* Aag2 cells (Fig. 4G). Luciferase
215 expression from direct translation of the transfected replicon RNA was similar in cells treated with

Loqs dsRNA or control dsRNA, whereas luciferase expression was blocked upon treatment with the translation inhibitor cycloheximide, as expected. These results suggest that Loqs does not affect viral RNA stability and translation efficiency, but that it is required for viral RNA replication.

As Loqs has been described as a co-factor of the siRNA pathway, it is unlikely that its proviral phenotype is dependent on RNAi. To directly test this, we next sequenced small RNAs produced in *Loqs*-depleted Aag2 cells infected with DENV or ZIKV. To account for differences in virus accumulation upon *Loqs* silencing, virus-derived siRNA (vsiRNA) levels were normalized to virus RNA levels in the same RNA used for small RNA sequencing. Despite efficient silencing of *Loqs* expression (Fig. S1D) and consequent reduction of viral RNA levels, no differences were observed in DENV or ZIKV-derived vsiRNA (Fig. 4H-I). Moreover, we did not observe major differences in miRNA levels (Fig. S1E-F), as also observed previously when both isoforms were depleted [24]. These results indicate that the proviral activity of Loqs is independent of its function in the RNAi pathway.

Loquacious colocalizes with dsRNA in viral replication organelles

Considering that Loqs contains multiple dsRBD domains, we explored the potential role of Loqs as a cofactor of viral RNA replication. We analyzed subcellular expression of Loqs-PA and Loqs-PB in mock- and DENV infected Aag2 cells (Fig. 5A). In non-infected cells, GFP-tagged Loqs-PA or Loqs-PB showed a discrete, punctate staining across the cytoplasm as well as lower, diffuse staining in the cytoplasm. In DENV-infected cells, both Loqs isoforms likewise showed a punctate pattern, but the signal was strongly focused in perinuclear punctae and this relocalization seemed to be more apparent for Loqs-PA. Importantly, for both isoforms a strong colocalization with viral

238 dsRNA was observed, suggesting that Loqs relocalizes to viral replication organelles in infected
239 cells (Fig. 5B).
240 We next investigated whether Loqs directly interacts with DENV RNA. To this end, we purified
241 recombinant Loqs-PA and Loqs-PB as a fusion protein with maltose binding protein (Fig. S2A)
242 and performed electrophoretic mobility shift assays (EMSA). As expected, Loqs-PA and Loqs-PB
243 bound with high affinity (5-40 nM) to control dsRNA in gel mobility shift assays (Fig. S2B). We
244 next incubated Loqs with *in vitro* transcribed RNA corresponding to the 5' untranslated region
245 (UTR), the 3'UTR, as well as coding sequences (in the NS1 and NS5 genes) and complexes were
246 resolved on native polyacrylamide gels. We found that both Loqs isoforms bound with high
247 affinity (95-191 nM) to the DENV 3'UTR, whereas binding to the other RNAs was much less
248 efficient (Fig. 5). Interestingly, multiple Loqs-3'UTR complexes were formed at higher Loqs
249 concentrations, suggesting that Loqs may bind to multiple RNA structures in the 3' UTR.
250 Altogether, we propose that DENV non-structural proteins recruit Loqs to viral replication
251 organelles, where it interacts through its dsRNA-binding motifs with viral RNA to facilitate viral
252 RNA replication.
253

DISCUSSION

Arboviruses replicate efficiently in their invertebrate vector as well as in their vertebrate hosts, and viral RNA and proteins thus interact with cellular proteins from these evolutionary diverse hosts. In this study, we used a proteomic approach to identify proteins interacting with DENV NS1 and NS5 in *Aedes* mosquitoes. Among the interactors, we identified the dsRNA binding protein Loquacious as a proviral factor for DENV and ZIKV that interacts with viral RNA at the 3' UTR. We propose that Loquacious is recruited to replication organelles to facilitate viral RNA replication. Loquacious is a cofactor of RNA silencing pathways [24] and our data thus suggest that DENV exploits proteins of an antiviral immune response for its own benefit. The human Loqs ortholog TARBP2 (also known as TRBP), a cofactor for HIV-1 replication that binds to the structured TAR RNA element [38], has been found to weakly interact with DENV NS1 [10], suggesting that the interaction may play a role in both mammals and mosquitoes.

Like in *Drosophila* [25–27], there seems to be functional specialization among the three *Loqs* paralogs in *Aedes* mosquitoes. Loqs-PA was proposed to be essential for miRNA function, whereas R2D2 and Loqs-PB are involved in siRNA production, although their relative importance could not be fully resolved [24]. Later, it was found that *Aedes* encodes another paralog, *Loqs2*, the product of which interacts with both R2D2 and Loqs, and is essential for antiviral defence [23]. Interestingly, *Loqs2* has a more restricted expression than *R2D2* and *Loqs* and it is not expressed in the midgut, the site of initial replication of arboviruses in the mosquito, whereas other RNAi pathway genes, including *Loqs* and *R2D2* are. Three *Loqs* isoforms are annotated in the current *Ae. aegypti* reference genome (AaegL5), of which the isoform with only two dsRBD, *Loqs-RC*, is only lowly expressed and did not affect DENV replication in our experiments. We recovered one peptide specific to isoform Loqs-PA in the NS1 interactome and *Loqs-RA* silencing reduced DENV

277 replication. However, we expect Loqs-PB to be proviral as well, as it bound DENV RNA and
278 localized to replication organelles to a similar extent as Loqs-PA.
279 As expected, Loqs interacted efficiently with dsRNA, but we found it to also interact with high
280 affinity with single-stranded RNA corresponding to the DENV 3' UTR. The 3' UTR is extensively
281 structured in diverse stem-loop structures, including pseudoknots (PK1 and PK2), dumbbell-like
282 structures (DB1 and DB2), as well as a long 3′ stem-loop (3′ SL) [39,40]. The 3' SL is essential
283 for viral RNA replication by mediating RNA-RNA interactions between the 5' and 3' ends of the
284 genome. Specifically, interaction of a cyclization sequence upstream of the initiator AUG, called
285 the upstream AUG region (5' UAR), with a complementary sequence in the stem of the 3' SL (3'
286 UAR) and mediates genome circularization that is required for initiation of negative strand RNA
287 synthesis [41,42]. It is likely that interaction of Loqs with the 3' UTR affects accessibility or
288 stability of RNA structures or the transition between linear and circularized states of the DENV
289 genome akin to the role of eukaryotic translation elongation factor (eIF1A) that interacts with the
290 3'SL to mediate flavivirus negative strand synthesis in mammals [43].
291 NS1 interacts with other viral non-structural proteins, is essential for early events in viral RNA
292 replication and replication organelle formation, and colocalizes with viral dsRNA [12,44,45]. We
293 identified Loqs as an interactor of NS1, expressed as part of a polyprotein with other non-structural
294 proteins flanked by non-viral UTRs, suggesting that Loqs was recruited to NS1 via protein-protein
295 interactions. In contrast, Loqs was not identified in the interactome of NS1 expressed individually
296 in mosquito cells [32]. Given that NS1 is an ER resident protein that is secreted through the
297 secretory pathway [46,47] and Loqs is a cytoplasmic protein, the interaction of Loqs with NS1 is
298 likely to be an indirect one. We suggest that the interaction is mediated by other viral non-structural
299 proteins interacting with NS1.

In addition to Loqs, we found multiple other interactors of NS1 and NS5 that merit further investigation, including the putative pro- and antiviral factors identified in the functional screen. Proviral E3 ubiquitin-protein ligase HYD (UBR5) was recently identified as a proviral host factor of ZIKV in a capsid interactome in mosquitoes [48], and the human ortholog UBR5 was also found to interact with DENV NS5 [13], suggesting HYD/UBR5 to be a broad cofactor for flaviviruses. The independent pull-down of HYD with the capsid and NS5 proteins in, respectively, the Gestuveo *et al.* study [13] and the present study suggests a prominent role of ubiquitin metabolism in flavivirus replication in mosquitoes. The identification of several proteins associated with ubiquitin metabolism (proteasome subunits β1, β2, α5 and α6, piccolo, mahjong and proviral muskelin) in NS5 immunoprecipitations agrees with previous reports suggesting that NS5 functions as an adaptor for the ubiquitination system, as it interacts with several E3-ligases in humans, including UBR4 to promote the degradation of STAT2 [13,49].

Among the potential antiviral factors from our screen are RNA binding proteins DIP1, an ortholog of human ADAR proteins to which pro- and antiviral activities have been attributed [50,51], and RPL12 (RPA12), which could modulate viral replication through its dsRNA cleavage and transcriptional termination activities [52]. In addition, we found the ER retention protein RER1 involved in protein degradation via the proteasome [53] and the chaperone protein HSP60A [54] to be antiviral factors, possibly related to a role of the stress response in antiviral immunity [55]. Yet, these observations need further investigation, especially since chaperone proteins, including HSP60, were proposed as flavivirus proviral cofactors in mammals [56,57]. We found a subunit of the OST complex, OstΔ (RPN2), to be antiviral activity in mosquito cells, which is in stark contrast to the proviral activity of the OST complex in mammals [10,58,59]. The OST complex

323 has previously been associated with the immune response [60,61] and could represent a host factor
324 with different activities in vertebrate and invertebrate hosts.
325 Viruses recruit host factors for viral replication and several dsRNA binding proteins have been
326 shown to interact with the 3'UTR of flaviviruses [62,63]. Despite its role as a regulator of RNAi
327 pathways central to antiviral immunity, our work establishes that the RNA binding protein Loqs
328 is hijacked through protein-protein and protein-RNA interactions to promote flavivirus replication
329 in mosquitoes. Our study provides novel insights into the mechanisms of replication of pathogenic
330 flaviviruses and identifies Loqs as a potential target to develop strategies to block flavivirus
331 transmission by vector mosquitoes.
332

METHODS

Cells and viruses

Aedes albopictus C6/36 (ECACC General Cell Collection, #89051705), U4.4 (kindly provided by Gorben Pijlman, Wageningen University, the Netherlands) and *Aedes aegypti* Aag2 (kindly provided by Raul Andino, University of California San Francisco) cells were maintained at 27°C in Leibovitz L15 medium (Gibco) supplemented with 10% heat inactivated fetal calf serum (FCS, PAA), 2% tryptose phosphate broth solution (Sigma), 1x MEM non-essential amino acids (Gibco), and 50 U/ml penicillin and 50 µg/ml streptomycin (Gibco).

DENV serotype 2 (DENV2, strain 16681) was provided by Beate Kümmerer (University of Bonn). ZIKV (strain H/PF/2013) was obtained from the European Virus Archive (EVAg, catalog number 001v-EVA1545). Virus stocks were prepared on C6/36 cells and titrated by end-point dilution on Vero FM cells. All viral infections were performed at an MOI of 0.1 in L15 medium without FCS and the medium was refreshed at 1 h post-infection with supplemented medium, containing 2% FCS.

Plasmids

DENV2 (strain NGC) non-structural genes were PCR amplified in three fragments from the pRepDVRluc plasmid [37] and all fragments were inserted into the PUb-MCS-2A-Puro plasmid [64] using In-Fusion cloning kit (Takara) to generate the PUb-NS(Ø) plasmid. PUb-NS(Ø) was subsequently mutated by site-directed mutagenesis to insert a cassette containing AgeI and SphI restriction sites. A 3xFLAG tag was then inserted by In-Fusion ligation of annealed oligos either at the N-terminus of NS1 to generate plasmid PUb-NS(1F) or at the C-terminus of NS5 to generate PUb-NS(5F). A PUb-GFP plasmid was generated by removing the Gateway cassette in the pUGW

vector [64], followed by the introduction of restriction sites for SphI, AvrII, AflII and NheI included in primers. *Ae. aegypti Loqs-RA* and *Loqs-RB* sequences (AaegL5) were cloned from the plasmids PUb-HA-Loqs-PB and PUb-HA-Loqs-PA (AaeL3), kindly provided by Zach Adelman (Texas A&M University) [24]. Loqs isoforms were inserted using the In-Fusion cloning kit into the PUb-GFP plasmid to express recombinant proteins with a GFP tag at the C-terminus and generate plasmids PUb-Loqs-PA-GFP and PUb-Loqs-PB-GFP, or into the pMal-C2X (NEB) to express recombinant proteins with a maltose-binding protein (MBP) tag at the N-terminus and generate pMal-Loqs-PA and pMal-Loqs-PB.

Primers used for cloning are listed in Table S3.

Immunoprecipitation

For standard immunoprecipitation, C6/36 cells were seeded in a 60 mm culture dish and incubated for 24 h. Cells were then transfected with 10 mg of PUb-NS(Ø), PUb-NS(1F) or PUb-NS(5F) and 20 µl of X-tremeGENE HP (Roche) and medium was refreshed after 3 hours. At 24 h after transfection, cells were harvested and washed in ice-cold PBS using 5 min centrifugations at 900 x *g*. Cell pellets were resuspended in 400 µL lysis buffer (10 mM Tris/Cl pH 7.4, 150 mM NaCl, 0.5 mM EDTA, 0.5% NP-40, 1x protease inhibitor cOmplete (Roche)). Samples were incubated with end-over-end rotation for 1 h at 4°C and followed by centrifugation at 18,000 x *g* for 30 min at 4°C. Total protein extracts were collected, diluted with 600 µL of dilution buffer (lysis buffer without NP-40) and incubated with 25 µL of pre-washed Anti-FLAG M2 Magnetic Beads (Sigma) on a rotor overnight at 4°C. The beads were washed three times in ice-cold dilution buffer, eluted in 50 µL of 2X SDS containing 5% β-mercaptoethanol at 95 °C for 10 min and analysed by western blot.

For mass spectrometry, immunoprecipitation was performed as described above, with the following modifications. C6/36 cells were seeded in 150 mm culture dishes (four dishes per condition) and transfected with 30 µg of plasmid and 60 µl of X-tremeGENE HP per dish. Cells were harvested at 24 h after transfection and washed in 5 mL of ice-cold PBS and cell pellets were resuspended in 2 mL of lysis buffer. Total protein extracts were diluted with 3 mL of dilution buffer and protein concentrations were estimated using the BCA Protein Assay (Pierce). 6 mg of total protein extract was incubated with 40 µL of Anti-FLAG M2 Agarose Beads (Sigma) and beads were washed a total of five times (three times in ice-cold dilution buffer and twice in ice-cold PBS), followed by on-bead trypsin digestion prior to MS analysis, as previously described [65]. For each condition, three biological replicates were used.

Western blotting

Protein samples were separated at 120 mV in 7.5% polyacrylamide gels for 90 min and transferred at 80 mA to PVDF membranes overnight at 4 °C using Bio-Rad systems. Proteins were labeled with primary antibodies diluted at 1:1000, mouse anti-FLAG M2 (Sigma, F1804) and rat anti-tubulin-α (MCA78G), and secondary antibodies diluted at 1:10,000, IRDye 800 goat anti-rat (Li-Cor, 926-32219) and IRDye 680RDye goat anti-mouse (Li-Cor, 926-32220). Western blots were imaged on the Odyssey CLx System (ThermoFischer).

Sample preparation and mass spectrometry

Samples were subjected to on-bead digestion [66], as follows: 50 µl of Elution buffer (EB: 2M urea, 100 mM Tris-pH 8.0 and 10 mM DTT) was added to each sample and incubated for 20 min at room temperature. Cysteines were alkylated using 50 mM iodoacetamide for 10 min, after which

0.25 µg of MS-grade trypsin (Promega) was added per sample. After 2 h incubation in a thermoshaker at room temperature, the supernatants were collected. Beads were washed once with 50 µl EB to collect as many peptides as possible, and this supernatant was combined with the first, after which 0.1 µg trypsin was added and samples were incubated overnight. The next day, samples were subjected to STAGE-tipping [67]. Tiny discs of C18 material were fixated in p200 tips. The C18 material was activated using methanol, and then thoroughly washed 1x with buffer B (80% acetronitrile, 0.1% TFA) and 2x with buffer A (0.1% TFA), after which the samples were loaded. Salts from the digestion buffer were washed away by an additional buffer A wash. Samples were eluted using buffer B for measurements.

Flag-immunoprecipitated samples were analyzed using reverse phase chromatography on an EASY-nLC1000 instrument coupled online to a Thermo Exploris 480 mass spectrometer. A 60 min gradient of buffer B (80% acetonitrile, 0.1% TFA) was applied to gradually release peptides from the C18 column into the mass spectrometer, which was ran at Top20 mode. A dynamic exclusion list was enabled for 30 proteins for 45 seconds after first occurrence. Only peptide ions with a charge between 2 and 6 were selected for fragmentation.

Mass spectrometry data analysis

The raw mass spectrometry data were analyzed using MaxQuant version 1.6.0.1 [68] and a database for *Ae. albopictus* (Aalbo_primary.1, RefSeq assembly: GCF_006496715.1) and DENV 16681 proteins). In addition to default settings, Deamidation (NQ) was used as a variable modification, and LFQ and iBAQ were enabled. Perseus [69] was used for filtering. Contaminants, reverse hits and hits with less than one peptide were removed. LFQ-values were subsequently log2-transformed and samples were divided into triplicates and filtered to have at least 3 valid

values in one group of replicates. The missing data were imputed using default settings. Students *t*-tests were performed for each of the baits compared to the control. R was used to visualize the data in volcano plots and a heatmap. When available, names of the closest ortholog from *D. melanogaster* as indicated in VectorBase were used to refer to mosquito proteins.

The mass spectrometry proteomics data have been deposited to the ProteomeXchange Consortium via the PRIDE partner repository [70] with the dataset identifier PXD031112. In the PRIDE accession, samples are referred to as "control", "1_flagip" and "5_flagip" for NS(Ø), NS(1F) and NS(5F), respectively.

Immunofluorescence assay

C6/36 cells were seeded on coverslips in 24-well plates 24 h before introducing transgenes. Cells were transfected with 1 µg of Pub-NS(Ø), Pub-NS(1F) or Pub-NS(5F) using 1 µL of X-tremeGENE HP (Roche) and incubated for 3 h before refreshing the medium. For infection experiments, Aag2 cells were infected 24 h after plating with DENV2 or mock for 72 h before transfection with Pub-Loqs-PA-GFP, Pub-Loqs-PB-GFP. At 24 h after transfection, cells were washed with PBS and fixed in 2% paraformaldehyde for 15 min at 4°C. Samples were further treated at room temperature and washed in PBS containing 0.05% Tween-20 between each of the following step. Cells were permeabilized with 0.1% Triton-X100 in PBS and treated with blocking buffer (2% BSA, 2% normal goat serum, 0.1% Triton, 0.05% Tween-20, 100 mM glycine in PBS) for 30 min. Samples were stained with primary mouse antibodies anti-FLAG M2 (Sigma, F1804) or anti-dsRNA J2 (Jena Bioscience, RNT-SCI-10010500), followed by secondary goat anti-mouse antibodies conjugated with Alexa Fluor 488 (ThermoFisher, A11001) or Alexa Fluor 594 (ThermoFisher, A11005). All antibodies were diluted 1:200 in blocking buffer. Nuclei were

448 stained with hoechst (5 µg/ml) for 15 min. Slides were mounted in Mowiol and stored at 4°C
449 before imaging.
450 Confocal images were acquired using a Zeiss LSM900 microscope and analysed with Icy ICY
451 Imaging [71]. Uncropped images are shown in Fig. S4.
452
453 **Bioinformatic analysis**
454 The interaction network for proteins of interest was predicted with STRING v10 [72], considering
455 a medium confidence (0.4) and a false discovery rate stringency of 5%, using the following four
456 sources: *text mining*, *experiments*, *databases* or *co-expression*. The network was visualized with
457 Cytoscape [73] with thickness of the edges relative to the number of sources supporting the
458 information. The genes enriched with NS1 and NS5 were separately analyzed with DAVID 6.8
459 [74] to identify enrichments for specific GO terms from the "biological process'' (BP) category,
460 using p-value < 0.1 as cutoff and containing at least 3 members per group. The complete GO term
461 analysis is presented in Table S2.
462 Sequences of Loqs isoforms and orthologs were aligned using MUSCLE [75], alignments were
463 curated with Gblocks [76] and a maximum likelihood phylogenetic tree was built with PhyML and
464 aLRT [77] using phylogeny.fr [78]. The phylogenetic tree was then visualized on iTOL [79].
465 Percentage identity were determined with Mview [80]. Reference sequences used are listed in
466 Table S4.
467
468 ***In vitro* transcription of replicon, dsRNA and EMSA probes**
469 The pRepDV2Rluc plasmid [37] was linearized with XbaI and used as template for *in vitro*
470 transcription of replicon RNA using the T7 RiboMAX Large Scale RNA Production System

(Promega) in the presence of Ribo m7G Cap Analog (Promega) at a cap analog to GTP ratio of 2.5. Replicon RNA was purified with the Rneasy Mini Kit (QIAGEN).

Templates for *in vitro* transcription of gene-specific 300-500 nt dsRNA and DENV2 EMSA probes were generated by PCR introducing a T7 promoter sequence or a universal tag at both 5' and 3' ends using the GoTaq Flexi DNA Polymerase (Promega). If present, the universal tag was then used in a second PCR to add T7 promoter sequences at both ends of the amplicon. T7 PCR products were used as a template for *in vitro* transcription by T7 RNA polymerase for 4 h at 37 °C. RNA for dsRNA was denatured at 95 °C for 10 min and gradually cooled to room temperature for annealing. Annealed dsRNA and EMSA probed were purified with the GenElute Mammalian Total RNA Miniprep Kit (Sigma) and quantified with the Nanodrop-1000 Spectrophotometer (ThermoFisher).

Primers used for in vitro transcription are listed in Table S3.

dsRNA-mediated gene silencing

Aag2 or U4.4 cells were plated in 48-well plates and transfected with 100 ng of dsRNA per well using 0.4 µL of X-tremeGENE HD (Roche). The medium was refreshed after 3 h and cells were incubated for 48 h. For infections, cells were transfected again with dsRNA as described above, incubated for 3 h, and then infected with DENV. Cells were harvested at the indicated time points for total RNA isolation using RNA-Solv (Omega Bio-tek). For replicon assays, Aag2 and U4.4 cells were transfected with 100 ng dsRNA and 250 ng RepDV2Rluc RNA per well using the TransIT-mRNA transfection kit (Mirus). As a positive control, cells transfected with RepDV2Rluc RNA in the absence of dsRNA were treated with 50 µM cycloheximide (CHX) at 1 h post-transfection. Proteins were harvested in passive lysis buffer 1x (Promega) at indicated times and

494 Renilla luciferase activity was measured using the Renilla-Glo Luciferase Assay system
495 (Promega).
496
497 **Reverse transcription and quantitative PCR**
498 Transcript annotation according to the reference genome AaegL5.2 was used to generate PCR
499 primers. For RT-qPCR, 200-500 ng of total RNA were treated with DNaseI (Ambion) for 45 min
500 at 37°C and then incubated with 2.5 mM EDTA for 10 min at 75°C. Total RNA was reverse
501 transcribed using the Taqman reverse transcription kit (Applied Biosystems). Relative quantitative
502 PCR analysis was performed using the GoTaq qPCR SYBR mastermix (Promega) on a
503 LightCycler 480 instrument (Roche). Target gene expression levels were normalized to the
504 expression of the housekeeping gene, *lysosomal aspartic protease* (LAP) for *Ae. aegypti* or
505 *ribosomal protein L5* (RPL5) for *Ae. albopictus*, and fold changes were calculated using the using
506 the 2(-ΔΔCT) method [81].
507 Primers used for in vitro transcription are listed in Table S3.
508
509 **Preparation of small RNA libraries**
510 Small RNA deep sequencing libraries were generated using the NEBNext Small RNA Library
511 Prep Set for Illumina (E7560, New England Biolabs), using 1 µg RNA as input. Libraries were
512 prepared in accordance with the manufacturer's instructions and sequenced on an Illumina
513 Hiseq4000 by the GenomEast Platform (Strasbourg, France).
514
515 **Small RNA sequence analysis**

516 The initial quality control was performed using FastQC and 3' adapters were trimmed using
517 cutadapt [82]. Small RNA sequences in the size range of 21-23 bp were considered as siRNA and
518 25-32 bp considered as piRNA. Subsequently, reads were uniquely mapped to the corresponding
519 virus genome, DENV2 (NCBI Reference Sequence: NC_001474.2) or ZIKV (GenBank:
520 KJ776791.2), allowing a maximum 1 mismatch. Samtools were used to quantify piRNA mapped
521 to the tapiR1 locus. To compare the vsiRNA changes upon *Loqs* silencing, uniquely mapped
522 siRNA reads were normalized to piRNAs mapped to the tapiR1 locus [83] to account for
523 differences in library size, and then normalized to DENV or ZIKV RNA copies based on RT-
524 qPCR performed on the same RNA as was used for small RNA sequencing.
525 Small RNA sequences in the size range of 19-25 nt were mapped to *Aedes* mature miRNA and
526 pre-miRNA sequences using Bowtie [84], allowing a maximum of 1 mismatch. miRNA sequences
527 and accession numbers were from the miRBase repository [85]. To compare total miRNA changes
528 upon dsLoqs, miRNA reads were normalized to piRNA mapped to the tapiR1 locus or total small
529 RNA library size. Samtools were used to quantify miRNA counts per sample [86]. DEseq2 was
530 used for differential analysis of miRNA between samples [87].
531
532 **Production and purification of recombinant protein**
533 *E. coli* strain XL10 Gold were transformed with plasmids encoding MBP-Loqs-PA or MBP-Loqs-
534 PB and cultured until midlog phase (OD_{600} of 0.6). Expression of recombinant proteins was then
535 induced with 1 mM isopropylβ-D-1-thiogalactopyranoside (IPTG) and cells were cultured
536 overnight at 27 °C. Cells were pelleted (13,000 x g, 15 min) and resuspended in E. coli Lysis
537 Buffer (PBS, 0.5% (w/v) Tween-20, 1 mM EDTA, 1x protease inhibitor cOmplete). Cells were
538 subjected to three freeze (-80 °C) / thaw (37 °C) cycles and sonicated (Branson Sonifier 250, 10

539 seconds, 3 x 5 cycles) before clearing debris by centrifugation at 13,000 x g for 30 min.
540 Recombinant proteins were affinity-purified using amylose resin using the manufacturer's protocol
541 (NEB) and eluted with 20 mM maltose. Protein concentration was measured in eluate fractions by
542 a Bradford assay (Bio-Rad) and the fractions with the highest concentration were transferred in a
543 Slide-A-Lyzer dialysis cassette (Thermo Fisher) and dialyzed to buffer (20 mM Tris-HCl pH 7.4,
544 0.5 mM EDTA, 5 mM MgCl2, 1 mM DTT, 140 mM NaCl, 2.7 mM KCl). Protein concentration
545 was determined by a Bradford assay. Recombinant proteins were snap-frozen in liquid nitrogen
546 and stored at -80°C in dialysis buffer with 30% glycerol.
547
548 **Electrophoretic mobility shift assays (EMSA)**
549 The synthesized probes were treated with DNaseI (Promega), dephosphorylated (Roche) and end-
550 labeled using T4 polynucleotide kinase (NEB) with [γ-^{32}P] ATP (Perkin Elmer). Unincorporated
551 nucleotides were removed with MicroSpin G-50 columns (Illustra). Samples were then heated for
552 5 min at 85°C, cooled to room temperature and incubated for 20 min in RNA folding buffer (111
553 mM HEPES, 6.7 mM $MgCl_2$, 111 mM NaCl). Purified proteins were diluted in dialysis buffer and
554 incubated for 30 min at room temperature with 1-10 ng of the labeled RNA in binding buffer (5
555 mM HEPES, 25 mM KCl, 2 mM MgCl2, 3.8% glycerol) in the presence of 0.625 mg/mL yeast
556 tRNA (Sigma). The reactions were loaded on a 6% native acrylamide gel and run at 4 °C. The
557 radioactive signal was quantified using a phosphor screen and a Typhoon FLA 7000 biomolecular
558 imager. RNA_{total} and RNA_{free} were quantified using Fiji [88] to determine the fraction bound = 1
559 − (RNA_{free}/RNA_{total}). Binding isotherms were fitted using specific binding with Hill slope in
560 GraphPad Prism7.
561

Statistical analysis

Graphical representation and statistical analyses were performed using GraphPad Prism7 software.

Differences were tested for statistical significance using unpaired two-tailed t-tests.

566 ACKNOWLEDGEMENTS

567 We thank members of the laboratory for discussions. We thank Pascal Jansen for processing the
568 mass spectrometry samples. We thank Zach Adelman (Texas A&M University) for kindly
569 providing Loqs expression plasmids and Beate Kümmerer (University of Bonn) for providing
570 DENV2 stock. ZIKV isolate H/PF/2013 was provided by Xavier de Lamballerie (Aix Marseille
571 Université) through the European Virus Archive (EVAg), funded by the European Union's
572 Horizon 2020 programme. The Vermeulen lab is part of the Oncode Institute, which is partly
573 funded by the Dutch Cancer Society. This study was financially supported by ZonMW within the
574 Off-Road program (grant number 04510011910045 to BB) and by a VICI grant from the Dutch
575 Research Council (NWO; grant number 016.VICI.170.090 to RPvR).

576

577 AUTHOR CONTRIBUTIONS

578 **Conceptualization:** Benoit Besson, Ronald van Rij

579 **Data curation: -**

580 **Formal analysis:** Benoit Besson, Jieqiong Qu, Ronald van Rij

581 **Funding acquisition:** Benoit Besson, Ronald van Rij

582 **Investigation:** Benoit Besson, Oscar M. Lezcano, Gijs Overheul, Kirsten Jansen, Cornelia G.

583 Spruijt, Jieqiong Qu

584 **Methodology:** Benoit Besson, Gijs Overheul, Cornelia G. Spruijt, Jieqiong Qu, Ronald van Rij

585 **Project administration:** Benoit Besson, Ronald van Rij

586 **Resources:** Michiel Vermeulen, Ronald van Rij

587 **Software:** -

588 **Supervision:** Benoit Besson, Michiel Vermeulen, Ronald van Rij

589 **Visualization:** Benoit Besson, Cornelia G. Spruijt, Oscar M. Lezcano, Gijs Overheul, Kirsten

590 Jansen, Jieqiong Qu

591 **Writing – original draft:** Benoit Besson, Ronald van Rij

592 **Writing – review & editing:** Benoit Besson, Jieqiong Qu, Ronald van Rij

593

594

595 REFERENCES

596 1. Bhatt S, Gething PW, Brady OJ, Messina JP, Farlow AW, Moyes CL, et al. The global
597 distribution and burden of dengue. Nature. 2013;496: 504–507. doi:10.1038/nature12060
598 2. Fischer D, Thomas SM, Neteler M, Tjaden NB, Beierkuhnlein C. Climatic suitability of
599 Aedes albopictus in Europe referring to climate change projections: comparison of
600 mechanistic and correlative niche modelling approaches. Eurosurveillance. 2014;19.
601 doi:10.2807/1560-7917.ES2014.19.6.20696
602 3. Aranda C, Martínez MJ, Montalvo T, Eritja R, Navero-Castillejos J, Herreros E, et al.
603 Arbovirus surveillance: first dengue virus detection in local aedes albopictus mosquitoes
604 in Europe, Catalonia, Spain, 2015. Eurosurveillance. 2018;23: e08347. doi:10.2807/1560-
605 7917.ES.2018.23.47.1700837
606 4. Kraemer MUG, Reiner RC, Brady OJ, Messina JP, Gilbert M, Pigott DM, et al. Past and
607 future spread of the arbovirus vectors Aedes aegypti and Aedes albopictus. Nat Microbiol.
608 2019;4: 854–863. doi:10.1038/s41564-019-0376-y
609 5. Kraemer MUG, Sinka ME, Duda KA, Mylne AQN, Shearer FM, Barker CM, et al. The
610 global distribution of the arbovirus vectors Aedes aegypti and Ae. albopictus. Elife.
611 2015;4. doi:10.7554/eLife.08347
612 6. Wang W-H, Urbina AN, Lin C-Y, Yang Z-S, Assavalapsakul W, Thitithanyanont A, et al.
613 Targets and strategies for vaccine development against dengue viruses. Biomed
614 Pharmacother. 2021;144: 112304. doi:10.1016/j.biopha.2021.112304
615 7. Neufeldt CJ, Cortese M, Acosta EG, Bartenschlager R. Rewiring cellular networks by
616 members of the Flaviviridae family. Nat Rev Microbiol. 2018;16: 125–142.
617 doi:10.1038/nrmicro.2017.170

618 8. Bhatt P, Sabeena SP, Varma M, Arunkumar G. Current Understanding of the Pathogenesis
619 of Dengue Virus Infection. Curr Microbiol. 2021;78: 17–32. doi:10.1007/s00284-020-
620 02284-w
621 9. Glasner DR, Puerta-Guardo H, Beatty PR, Harris E. The Good, the Bad, and the
622 Shocking: The Multiple Roles of Dengue Virus Nonstructural Protein 1 in Protection and
623 Pathogenesis. Annu Rev Virol. 2018;5: 227–253. doi:10.1146/annurev-virology-101416-
624 041848
625 10. Hafirassou ML, Meertens L, Umaña-Diaz C, Labeau A, Dejarnac O, Bonnet-Madin L, et
626 al. A Global Interactome Map of the Dengue Virus NS1 Identifies Virus Restriction and
627 Dependency Host Factors. CellReports. 2017;21: 3900–3913.
628 doi:10.1016/j.celrep.2017.11.094
629 11. Shue B, Chiramel AI, Cerikan B, To T-H, Frölich S, Pederson SM, et al. Genome-Wide
630 CRISPR Screen Identifies RACK1 as a Critical Host Factor for Flavivirus Replication.
631 Pfeiffer JK, editor. J Virol. 2021;95. doi:10.1128/JVI.00596-21
632 12. Płaszczyca A, Scaturroid P, Neufeldtid CJ, Corteseid M, Cerikan B, Ferla S, et al. A novel
633 interaction between dengue virus nonstructural protein 1 and the NS4A-2K-4B precursor
634 is required for viral RNA replication but not for formation of the membranous replication
635 organelle. PLoS Pathog. 2019. doi:10.1371/journal.ppat.1007736
636 13. De Maio FA, Risso G, Iglesias NG, Shah P, Pozzi B, Gebhard LG, et al. The Dengue
637 Virus NS5 Protein Intrudes in the Cellular Spliceosome and Modulates Splicing. PLoS
638 Pathog. 2016;12: e1005841--29. doi:10.1371/journal.ppat.1005841
639 14. Shah PS, Link N, Jang GM, Sharp PP, Zhu T, Swaney DL, et al. Comparative Flavivirus-
640 Host Protein Interaction Mapping Reveals Mechanisms of Dengue and Zika Virus

641 Pathogenesis. Cell. 2018;175: 1931-1945.e18. doi:10.1016/j.cell.2018.11.028

642 15. Schneider WM, Hoffmann H-H. Flavivirus–host interactions: an expanding network of
643 proviral and antiviral factors. Curr Opin Virol. 2022;52: 71–77.
644 doi:10.1016/j.coviro.2021.11.007

645 16. Hoffmann H-H, Schneider WM, Rozen-Gagnon K, Miles LA, Schuster F, Razooky B, et
646 al. TMEM41B Is a Pan-flavivirus Host Factor. Cell. 2021;184: 133-148.e20.
647 doi:10.1016/j.cell.2020.12.005

648 17. Morchang A, Lee RCH, Yenchitsomanus PT, Sreekanth GP, Noisakran S, Chu JJH, et al.
649 RNAi screen reveals a role of SPHK2 in dengue virus–mediated apoptosis in hepatic cell
650 lines. PLoS One. 2017. doi:10.1371/journal.pone.0188121

651 18. Kwon Y-J, Heo J, Wong HEE, Cruz DJM, Velumani S, da Silva CT, et al. Kinome siRNA
652 screen identifies novel cell-type specific dengue host target genes. Antiviral Res.
653 2014;110: 20–30. doi:10.1016/j.antiviral.2014.07.006

654 19. Barrows NJ, Anglero-Rodriguez Y, Kim B, Jamison SF, Le Sommer C, McGee CE, et al.
655 Dual roles for the ER membrane protein complex in flavivirus infection: viral entry and
656 protein biogenesis. Sci Rep. 2019;9: 9711. doi:10.1038/s41598-019-45910-9

657 20. Bronkhorst AW, van Rij RP. The long and short of antiviral defense: small RNA-based
658 immunity in insects. Curr Opin Virol. 2014;7: 19–28. doi:10.1016/j.coviro.2014.03.010

659 21. Guo Z, Li Y, Ding S-W. Small RNA-based antimicrobial immunity. Nat Rev Immunol.
660 2019;19: 31–44. doi:10.1038/s41577-018-0071-x

661 22. Olson KE, Blair CD. Arbovirus–mosquito interactions: RNAi pathway. Curr Opin Virol.
662 2015;15: 119–126. doi:10.1016/j.coviro.2015.10.001

663 23. Olmo RP, Ferreira AGA, Izidoro-Toledo TC, Aguiar ERGR, de Faria IJS, de Souza KPR,

et al. Control of dengue virus in the midgut of Aedes aegypti by ectopic expression of the dsRNA-binding protein Loqs2. Nat Microbiol. 2018;3: 1385–1393. doi:10.1038/s41564-018-0268-6

24. Haac ME, Anderson MAE, Eggleston H, Myles KM, Adelman ZN. The hub protein loquacious connects the microRNA and short interfering RNA pathways in mosquitoes. Nucleic Acids Res. 2015;43: 3688–3700. doi:10.1093/nar/gkv152

25. Liu Q, Rand TA, Kalidas S, Du F, Kim H-E, Smith DP, et al. R2D2, a Bridge Between the Initiation and Effector Steps of the Drosophila RNAi Pathway. Science (80-). 2003;301: 1921–1925. doi:10.1126/science.1088710

26. Jiang F, Ye X, Liu X, Fincher L, McKearin D, Liu Q. Dicer-1 and R3D1-L catalyze microRNA maturation in Drosophila. Genes Dev. 2005;19: 1674–1679. doi:10.1101/gad.1334005

27. Förstemann K, Tomari Y, Du T, Vagin V V., Denli AM, Bratu DP, et al. Normal microRNA Maturation and Germ-Line Stem Cell Maintenance Requires Loquacious, a Double-Stranded RNA-Binding Domain Protein. Carrington JC, editor. PLoS Biol. 2005;3: e236. doi:10.1371/journal.pbio.0030236

28. Sánchez-Vargas I, Scott JC, Poole-Smith BK, Franz AWE, Barbosa-Solomieu V, Wilusz J, et al. Dengue Virus Type 2 Infections of Aedes aegypti Are Modulated by the Mosquito's RNA Interference Pathway. Rice CM, editor. PLoS Pathog. 2009;5: e1000299. doi:10.1371/journal.ppat.1000299

29. Miller S, Kastner S, Krijnse-Locker J, Bühler S, Bartenschlager R. The Non-structural Protein 4A of Dengue Virus Is an Integral Membrane Protein Inducing Membrane Alterations in a 2K-regulated Manner. J Biol Chem. 2007;282: 8873–8882.

687 doi:10.1074/jbc.M609919200

688 30. Choy MM, Zhang SL, Costa V V., Tan HC, Horrevorts S, Ooi EE. Proteasome Inhibition
689 Suppresses Dengue Virus Egress in Antibody Dependent Infection. Dinglasan RR, editor.
690 PLoS Negl Trop Dis. 2015;9: e0004058. doi:10.1371/journal.pntd.0004058

691 31. Kanlaya R, Pattanakitsakul S, Sinchaikul S, Chen S-T, Thongboonkerd V. The
692 Ubiquitin−Proteasome Pathway Is Important for Dengue Virus Infection in Primary
693 Human Endothelial Cells. J Proteome Res. 2010;9: 4960–4971. doi:10.1021/pr100219y

694 32. Carabello GI, Rosales R, Viettri M, Ding S, Greenberg HB, Ludert JE. The dengue virus
695 non-structural protein 1 (NS1) interacts with the putative epigenetic regulator DIDO1 to
696 promote flavivirus replication. bioRxiv. 2021. Available:
697 https://doi.org/10.1101/2021.09.01.458517

698 33. Wu D, Murashov AK. Molecular mechanisms of peripheral nerve regeneration: emerging
699 roles of microRNAs. Front Physiol. 2013;4. doi:10.3389/fphys.2013.00055

700 34. Li K, Phoo WW, Luo D. Functional interplay among the flavivirus NS3 protease, helicase,
701 and cofactors. Virol Sin. 2014;29: 74–85. doi:10.1007/s12250-014-3438-6

702 35. Lai H, Li C, Hong C, Sun H, Chiu C, Ou D, et al. <scp>TARBP</scp> 2-mediated
703 destabilization of Nanog overcomes sorafenib resistance in hepatocellular carcinoma. Mol
704 Oncol. 2019;13: 928–945. doi:10.1002/1878-0261.12449

705 36. Kurosaki T, Popp MW, Maquat LE. Quality and quantity control of gene expression by
706 nonsense-mediated mRNA decay. Nat Rev Mol Cell Biol. 2019;20: 406–420.
707 doi:10.1038/s41580-019-0126-2

708 37. van Cleef KWR, Overheul GJ, Thomassen MC, Kaptein SJF, Davidson AD, Jacobs M, et
709 al. Identification of a new dengue virus inhibitor that targets the viral NS4B protein and

restricts genomic RNA replication. Antiviral Res. 2013;99: 165–171. doi:10.1016/j.antiviral.2013.05.011

38. Sanghvi VR, Steel LF. The Cellular TAR RNA Binding Protein, TRBP, Promotes HIV-1 Replication Primarily by Inhibiting the Activation of Double-Stranded RNA-Dependent Kinase PKR. J Virol. 2011;85: 12614–12621. doi:10.1128/JVI.05240-11

39. Shivaprasad S, Sarnow P. The tale of two flaviviruses: subversion of host pathways by RNA shapes in dengue and hepatitis C viral RNA genomes. Curr Opin Microbiol. 2021;59: 79–85. doi:10.1016/j.mib.2020.08.007

40. Choi KH. The Role of the Stem-Loop A RNA Promoter in Flavivirus Replication. Viruses. 2021;13: 1107. doi:10.3390/v13061107

41. Gebhard LG, Filomatori C V., Gamarnik A V. Functional RNA Elements in the Dengue Virus Genome. Viruses. 2011;3: 1739–1756. doi:10.3390/v3091739

42. Villordo SM, Gamarnik A V. Genome cyclization as strategy for flavivirus RNA replication. Virus Res. 2009;139: 230–239. doi:10.1016/j.virusres.2008.07.016

43. Davis WG, Blackwell JL, Shi P-Y, Brinton MA. Interaction between the Cellular Protein eEF1A and the 3′-Terminal Stem-Loop of West Nile Virus Genomic RNA Facilitates Viral Minus-Strand RNA Synthesis. J Virol. 2007;81: 10172–10187. doi:10.1128/JVI.00531-07

44. Scaturro P, Cortese M, Chatel-Chaix L, Fischl W, Bartenschlager R. Dengue Virus Non-structural Protein 1 Modulates Infectious Particle Production via Interaction with the Structural Proteins. PLoS Pathog. 2015. doi:10.1371/journal.ppat.1005277

45. Mackenzie JM, Jones MK, Young PR. Immunolocalization of the Dengue virus nonstructural glycoprotein NS1 suggests a role in viral RNA replication. Virology. 1996.

733 doi:10.1006/viro.1996.0307

734 46. Alcalá AC, Medina F, González-Robles A, Salazar-Villatoro L, Fragoso-Soriano RJ,
735 Vásquez C, et al. The dengue virus non-structural protein 1 (NS1) is secreted efficiently
736 from infected mosquito cells. Virology. 2016;488: 278–287.
737 doi:10.1016/j.virol.2015.11.020

738 47. Gutsche I, Coulibaly F, Voss JE, Salmon J, D'Alayer J, Ermonval M, et al. Secreted
739 dengue virus nonstructural protein NS1 is an atypical barrel-shaped high-density
740 lipoprotein. Proc Natl Acad Sci. 2011;108: 8003–8008. doi:10.1073/pnas.1017338108

741 48. Gestuveo RJ, Royle J, Donald CL, Lamont DJ, Hutchinson EC, Merits A, et al. Analysis
742 of Zika virus capsid-Aedes aegypti mosquito interactome reveals pro-viral host factors
743 critical for establishing infection. Nat Commun. 2021;12: 2766. doi:10.1038/s41467-021-
744 22966-8

745 49. Morchang A, Lee RCH, Yenchitsomanus P, Sreekanth GP, Noisakran S, Chu JJH, et al.
746 RNAi screen reveals a role of SPHK2 in dengue virus–mediated apoptosis in hepatic cell
747 lines. Jin X, editor. PLoS One. 2017;12: e0188121. doi:10.1371/journal.pone.0188121

748 50. Pfaller CK, George CX, Samuel CE. Adenosine Deaminases Acting on RNA (ADARs)
749 and Viral Infections. Annu Rev Virol. 2021;8: 239–264. doi:10.1146/annurev-virology-
750 091919-065320

751 51. Samuel CE. Adenosine deaminases acting on RNA (ADARs) are both antiviral and
752 proviral. Virology. 2011. doi:10.1016/j.virol.2010.12.004

753 52. Płaszczyca A, Scaturro P, Neufeldt CJ, Cortese M, Cerikan B, Ferla S, et al. A novel
754 interaction between dengue virus nonstructural protein 1 and the NS4A-2K-4B precursor
755 is required for viral RNA replication but not for formation of the membranous replication

organelle. Randall G, editor. PLOS Pathog. 2019;15: e1007736. doi:10.1371/journal.ppat.1007736

53. Annaert W, Kaether C. Bring it back, bring it back, don't take it away from me – the sorting receptor RER1. J Cell Sci. 2020;133. doi:10.1242/jcs.231423

54. Caruso Bavisotto C, Alberti G, Vitale AM, Paladino L, Campanella C, Rappa F, et al. Hsp60 Post-translational Modifications: Functional and Pathological Consequences. Front Mol Biosci. 2020;7. doi:10.3389/fmolb.2020.00095

55. Merkling SH, Overheul GJ, van Mierlo JT, Arends D, Gilissen C, van Rij RP. The heat shock response restricts virus infection in Drosophila. Sci Rep. 2015;5: 12758. doi:10.1038/srep12758

56. Iyer K, Chand K, Mitra A, Trivedi J, Mitra D. Diversity in heat shock protein families: functional implications in virus infection with a comprehensive insight of their role in the HIV-1 life cycle. Cell Stress Chaperones. 2021;26: 743–768. doi:10.1007/s12192-021-01223-3

57. Padwad YS, Mishra KP, Jain M, Chanda S, Karan D, Ganju L. RNA interference mediated silencing of Hsp60 gene in human monocytic myeloma cell line U937 revealed decreased dengue virus multiplication. Immunobiology. 2009;214: 422–429. doi:10.1016/j.imbio.2008.11.010

58. Lin DL, Cherepanova NA, Bozzacco L, MacDonald MR, Gilmore R, Tai AW. Dengue Virus Hijacks a Noncanonical Oxidoreductase Function of a Cellular Oligosaccharyltransferase Complex. Lipkin WI, editor. MBio. 2017;8. doi:10.1128/mBio.00939-17

59. Płaszczyca A, Scaturro P, Neufeldt CJ, Cortese M, Cerikan B, Ferla S, et al. A novel

779 interaction between dengue virus nonstructural protein 1 and the NS4A-2K-4B precursor
780 is required for viral RNA replication but not for formation of the membranous replication
781 organelle. Randall G, editor. PLOS Pathog. 2019;15: e1007736.
782 doi:10.1371/journal.ppat.1007736
783 60. Jeong D-E, Lee Y, Ham S, Lee D, Kwon S, Park H-EH, et al. Inhibition of the
784 oligosaccharyl transferase in Caenorhabditis elegans that compromises ER proteostasis
785 suppresses p38-dependent protection against pathogenic bacteria. Garsin DA, editor.
786 PLOS Genet. 2020;16: e1008617. doi:10.1371/journal.pgen.1008617
787 61. Farid A, Malinovsky FG, Veit C, Schoberer J, Zipfel C, Strasser R. Specialized Roles of
788 the Conserved Subunit OST3/6 of the Oligosaccharyltransferase Complex in Innate
789 Immunity and Tolerance to Abiotic Stresses. Plant Physiol. 2013;162: 24–38.
790 doi:10.1104/pp.113.215509
791 62. Embarc-Buh A, Francisco-Velilla R, Martinez-Salas E. RNA-Binding Proteins at the
792 Host-Pathogen Interface Targeting Viral Regulatory Elements. Viruses. 2021;13: 952.
793 doi:10.3390/v13060952
794 63. Roby J, Pijlman G, Wilusz J, Khromykh A. Noncoding Subgenomic Flavivirus RNA:
795 Multiple Functions in West Nile Virus Pathogenesis and Modulation of Host Responses.
796 Viruses. 2014;6: 404–427. doi:10.3390/v6020404
797 64. Joosten J, Miesen P, Ta\c sköprü E, Pennings B, Jansen PWTC, Huynen MA, et al. The
798 Tudor protein Veneno assembles the ping-pong amplification complex that produces viral
799 piRNAs in Aedes mosquitoes. Nucleic Acids Res. 2019;47: 2546–2559.
800 doi:10.1093/nar/gky1266
801 65. Smits AH, Jansen PWTC, Poser I, Hyman AA, Vermeulen M. Stoichiometry of

chromatin-associated protein complexes revealed by label-free quantitative mass spectrometry-based proteomics. Nucleic Acids Res. 2013;41: e28–e28. doi:10.1093/nar/gks941

66. Baymaz HI, Spruijt CG, Vermeulen M. Identifying Nuclear Protein–Protein Interactions Using GFP Affinity Purification and SILAC-Based Quantitative Mass Spectrometry. Methods in Molecular Biology. 2014. pp. 207–226. doi:10.1007/978-1-4939-1142-4_15

67. Rappsilber J, Ishihama Y, Mann M. Stop and Go Extraction Tips for Matrix-Assisted Laser Desorption/Ionization, Nanoelectrospray, and LC/MS Sample Pretreatment in Proteomics. Anal Chem. 2003;75: 663–670. doi:10.1021/ac026117i

68. Cox J, Mann M. MaxQuant enables high peptide identification rates, individualized p.p.b.-range mass accuracies and proteome-wide protein quantification. Nat Biotechnol. 2008;26: 1367–1372. doi:10.1038/nbt.1511

69. Tyanova S, Temu T, Sinitcyn P, Carlson A, Hein MY, Geiger T, et al. The Perseus computational platform for comprehensive analysis of (prote)omics data. Nat Methods. 2016;13: 731–740. doi:10.1038/nmeth.3901

70. Perez-Riverol Y, Bai J, Bandla C, García-Seisdedos D, Hewapathirana S, Kamatchinathan S, et al. The PRIDE database resources in 2022: a hub for mass spectrometry-based proteomics evidences. Nucleic Acids Res. 2022;50: D543–D552. doi:10.1093/nar/gkab1038

71. de Chaumont F, Dallongeville S, Chenouard N, Hervé N, Pop S, Provoost T, et al. Icy: an open bioimage informatics platform for extended reproducible research. Nat Methods. 2012;9: 690–696. doi:10.1038/nmeth.2075

72. Szklarczyk D, Franceschini A, Wyder S, Forslund K, Heller D, Huerta-Cepas J, et al.

STRING v10: protein–protein interaction networks, integrated over the tree of life. Nucleic Acids Res. 2015;43: D447–D452. doi:10.1093/nar/gku1003

73. Shannon P, Markiel A, Ozier O, Baliga NS, Wang JT, Ramage D, et al. Cytoscape: A Software Environment for Integrated Models of Biomolecular Interaction Networks. Genome Res. 2003;13: 2498–2504. doi:10.1101/gr.1239303

74. Huang DW, Sherman BT, Lempicki RA. Systematic and integrative analysis of large gene lists using DAVID bioinformatics resources. Nat Protoc. 2009;4: 44–57. doi:10.1038/nprot.2008.211

75. Chacón J, Luebert F, Hilger HH, Ovchinnikova S, Selvi F, Cecchi L, et al. The borage family (Boraginaceae s.str.): A revised infrafamilial classification based on new phylogenetic evidence, with emphasis on the placement of some enigmatic genera. Taxon. 2016;65: 523–546. doi:10.12705/653.6

76. Castresana J. Selection of Conserved Blocks from Multiple Alignments for Their Use in Phylogenetic Analysis. Mol Biol Evol. 2000;17: 540–552. doi:10.1093/oxfordjournals.molbev.a026334

77. Anisimova M, Gascuel O. Approximate Likelihood-Ratio Test for Branches: A Fast, Accurate, and Powerful Alternative. Sullivan J, editor. Syst Biol. 2006;55: 539–552. doi:10.1080/10635150600755453

78. Dereeper A, Guignon V, Blanc G, Audic S, Buffet S, Chevenet F, et al. Phylogeny.fr: robust phylogenetic analysis for the non-specialist. Nucleic Acids Res. 2008;36: W465–W469. doi:10.1093/nar/gkn180

79. Letunic I, Bork P. Interactive Tree Of Life (iTOL) v5: an online tool for phylogenetic tree display and annotation. Nucleic Acids Res. 2021;49: W293–W296.

doi:10.1093/nar/gkab301

80. Brown NP, Leroy C, Sander C. MView: a web-compatible database search or multiple alignment viewer. Bioinformatics. 1998;14: 380–381. doi:10.1093/bioinformatics/14.4.380

81. Livak KJ, Schmittgen TD. Analysis of Relative Gene Expression Data Using Real-Time Quantitative PCR and the 2−ΔΔCT Method. Methods. 2001;25: 402–408. doi:10.1006/meth.2001.1262

82. Martin M. Cutadapt removes adapter sequences from high-throughput sequencing reads. EMBnet.journal. 2011;17: 10. doi:10.14806/ej.17.1.200

83. Halbach R, Miesen P, Joosten J, Taşköprü E, Rondeel I, Pennings B, et al. A satellite repeat-derived piRNA controls embryonic development of Aedes. Nature. 2020;580: 274–277. doi:10.1038/s41586-020-2159-2

84. Langmead B. Aligning Short Sequencing Reads with Bowtie. Curr Protoc Bioinforma. 2010;32. doi:10.1002/0471250953.bi1107s32

85. Kozomara A, Birgaoanu M, Griffiths-Jones S. miRBase: from microRNA sequences to function. Nucleic Acids Res. 2019;47: D155–D162. doi:10.1093/nar/gky1141

86. Li H, Handsaker B, Wysoker A, Fennell T, Ruan J, Homer N, et al. The Sequence Alignment/Map format and SAMtools. Bioinformatics. 2009;25: 2078–2079. doi:10.1093/bioinformatics/btp352

87. Love MI, Huber W, Anders S. Moderated estimation of fold change and dispersion for RNA-seq data with DESeq2. Genome Biol. 2014;15: 550. doi:10.1186/s13059-014-0550-8

88. Scaturro P, Cortese M, Chatel-Chaix L, Fischl W, Bartenschlager R. Dengue Virus Non-

structural Protein 1 Modulates Infectious Particle Production via Interaction with the Structural Proteins. Pierson TC, editor. PLOS Pathog. 2015;11: e1005277. doi:10.1371/journal.ppat.1005277

89. Akbari OS, Antoshechkin I, Amrhein H, Williams B, Diloreto R, Sandler J, et al. The Developmental Transcriptome of the Mosquito Aedes aegypti , an Invasive Species and Major Arbovirus Vector. G3 Genes|Genomes|Genetics. 2013;3: 1493–1509. doi:10.1534/g3.113.006742

90. Matthews BJ, Dudchenko O, Kingan SB, Koren S, Antoshechkin I, Crawford JE, et al. Improved reference genome of Aedes aegypti informs arbovirus vector control. Nature. 2018;563: 501–507. doi:10.1038/s41586-018-0692-z

91. Biedler JK, Hu W, Tae H, Tu Z. Identification of Early Zygotic Genes in the Yellow Fever Mosquito Aedes aegypti and Discovery of a Motif Involved in Early Zygotic Genome Activation. Aerts S, editor. PLoS One. 2012;7: e33933. doi:10.1371/journal.pone.0033933

887 LEGENDS

888 **Figure 1. Interactome of NS1 and NS5 in *Aedes* mosquito cells**

889 **A.** Schematic representation of constructs used to express DENV non-structural proteins in
890 mosquito cells. Constructs were generated with a 3xFLAG tag at the N-terminus of NS1 (NS(1F)),
891 the C-terminus of NS5 (NS(5F)). A construct without a tag (NS(ØF)) was included as a control.
892 2A, self-cleaving peptide from foot-and-mouth disease virus; PAC, Puromycin N-
893 acetyltransferase. **B.** Western blot of input and FLAG immunoprecipitation samples of C6/36 cells
894 expressing NS(ØF), NS(1F) and NS(5F), stained with FLAG and α-tubulin (Tub) antibodies. See
895 uncropped gel in Fig. S3. **C.** Confocal microscopy image of FLAG-tagged NS1 and NS5 in C6/36
896 cells at 24 h after transgene transfection. Cells were stained with anti-FLAG M2 antibody (green)
897 and Hoechst to stain nuclei (blue). **D.** Volcano plot of proteins interacting with 3xFLAG-tagged
898 NS1 (top) or NS5 (bottom) in C6/36 cell lysates as determined by label-free quantitative mass
899 spectrometry. The X-axis shows the log2 fold enrichment over untagged NS(ØF) (control), and
900 the Y-axis shows -log10(*p*-value). Proteins in the top right are identified as significantly enriched
901 proteins. Colored dots indicate proteins of interest. Each condition was performed in triplicate. **E.**
902 Heatmap of the relative enrichment (red) and depletion (blue) of proteins in each sample, based on
903 row-mean subtraction and K-means clustering. Statistical enrichment in the volcano plot analysis
904 in indicated. Ost48 and Stt3A were included, although not significantly enriched. 'Low' indicates
905 an enrichment between 2 and 2.5-fold, below the threshold of the volcano plot. **D-E** Colored dots
906 indicate proteins of interest.

907

908 **Figure 2. Characterization of DENV NS1 and NS5 interactomes**

909 **A.** Venn diagram of highlighting 85 interactors of NS1 and/or NS5 identified by mass
910 spectrometry. **B.** GO term analyses of interactors of NS1 (top panel) and NS5 (lower panel).
911 Enrichment of biological processes was based on *D. melanogaster* ortholog annotation. Numbers
912 indicate -$\log_{10}$ *p* values. See complete list of GO terms in Table S2. **C.** Functional STRING
913 networks based on *D. melanogaster* ortholog annotation. Hits were classified and colored
914 according to their enrichment in ≥2 out of 3 NS(1F) or NS(5F) samples in the heatmap of Fig. 1E.
915 Node sizes represent the fold enrichment in NS(1F) or NS(5F) immunoprecipitation, keeping the
916 highest value if the interactor was present in both. Edges are representative of the number of
917 sources (solid or dashed) and the confidence (color) supporting the interaction as defined by
918 STRING. Font indicates hits confirmed (bold) or not (italic) as modulators of DENV in the
919 functional screening (Fig. 3).
920
921 **Figure 3. Functional screen identifies Loqs as a DENV proviral host factor in *Aedes***
922 **mosquitoes**
923 **A.** Schematic outline of the functional RNAi screen. **B-C.** Relative quantification of target gene
924 expression (top panel) and DENV RNA levels (lower panel) in U4.4 cells upon silencing of the
925 indicated genes. Selected genes from the initial screen (B) were tested in an independent validation
926 screen (C) using dsRNA targeting a different region of the gene. Expression was quantified by
927 RT-qPCR, normalized to the house-keeping gene *ribosomal protein L5*, and expressed relative to
928 expression in cells treated with dsRNA targeting firefly luciferase (CTRL). *Ago2* was used as a
929 positive control. Data represent means and standard deviation of three replicates. Color coding
930 represents classification of hits based on gene knockdown efficiency, phenotype, and consistency
931 between screens. Light grey, inefficient knockdown (< 0.5-fold); dark grey, no phenotype despite

932 efficient knockdown (> 0.5-fold); dark red, strong hit with efficient knockdown, and DENV RNA
933 levels < 0.66-fold or >1.5-fold in both dsRNA sets; light red, weak hits for which one of the criteria
934 was not met. * $p < 0.05$; ** $p < 0.01$; *** $p < 0.001$; **** $p < 0.0001$
935
936 **Figure 4. Loquacious is an essential co-factor for flavivirus replication**
937 **A.** Structure of *Loquacious* splice variants in *Ae. aegypti* (DSRM, dsRNA-binding motif) and
938 maximum likelihood phylogenic tree based on the protein sequence of Loqs-PA and its orthologs
939 and paralogs. ce, *Caenorhabditis elegans*; dm, *Drosophila melanogaster*; h, *Homo sapiens*; aae,
940 *Ae. aegypti*; aal, *Ae. albopictus*. Percentages indicates the identity between protein sequences
941 compared to *Ae. aegypti* Loqs-PA. Branch lengths are proportional to the number of substitutions
942 per site. *Loqs* transcript annotation is according to the reference genome AaegL5, which differs
943 from the annotation used in [24]. **B.** Loqs peptides identified by mass spectrometry in NS1
944 immunoprecipitations. The peptide unique to Loqs-RB is indicated in blue; other peptides are
945 shared between *Loqs* isoforms. **C.** Loqs-RA and Loqs-RB-specific amplicons from PCR using
946 primers spanning exon 5 on cDNA from Aag2 cells. **D.** PCR amplification of *Loqs* splice variants
947 with various set of primers on cDNA or genomic DNA isolated from Aag2 cells. Numbers indicate
948 expected sizes. **E.** Relative quantification of DENV RNA at 72 h infection of Aag2 cells in which
949 siRNA and miRNA pathway genes were silenced. **F**. Relative quantification of DENV RNA (top
950 panel) or ZIKV RNA (lower panel) at the indicated time after infection in *Ago2* or *Loqs*-depleted
951 Aag2 cells. **G.** *Renilla* luciferase activity in Aag2 cells (left) and U4.4 cells (right) transfected with
952 DENV2 subgenomic replicon RNA and dsRNA targeting *Loqs* (dsLoqs) or firefly luciferase
953 (dsGL3) as a control. Luciferase activity was assessed at the indicated time points and normalized
954 to dsGL3-treated cells at 3 h after transfection. Cells treated with cycloheximide (CHX) were

included as control. **H-I.** Relative quantification of DENV (H) and ZIKV (I) RNA (left) and vsiRNA (right) 48h after infection at a MOI of 0.1 in *Loqs*-depleted or control (GL3 dsRNA treated) Aag2 cells. vsiRNA were normalized to cellular tapiR1 piRNA and viral RNA. **E-F, H-I.** Viral RNA levels were quantified by RT-qPCR, normalized to the housekeeping gene *lysosomal aspartic protease* and expressed relative to the expression in cells treated using dsRNA targeting luciferase (GL3) as negative control. See relative knockdown-target quantification in Supplementary Fig. S2. Bars represent mean and standard deviation from at least three biological replicates. * $p < 0.05$; ** $p < 0.01$; *** $p < 0.001$; **** $p < 0.0001$.

Figure 5. Loquacious colocalizes with DENV replication organelles

A. Confocal microscopy images of mock or DENV infected Aag2 cells. Cells were transfected at 72 h post infection with plasmids encoding the indicated transgenes or mock transfected (Ø) and processed for microscopy 24 h later. Cells were stained with anti-dsRNA J2 antibody (red) and Hoechst to stain nuclei (blue). Scale bar corresponds to 5 μm and is the same for all panels. In mock infected cells, a nuclear background signal is detectable that is distinct from the cytoplasmic viral dsRNA signal in DENV infected cells. **B.** Three-dimensional visualizations of two DENV infected Aag2 cells transfected with Loqs-PA-GFP indicated with a dashed square in panel A. The dsRNA and GFP signals were optimized for visualization in the three-dimensional projection. The grid is scaled with 2 μm xyz units.

Figure 6. Loquacious interacts directly with DENV 3'UTR

A. Electrophoretic mobility assay of *Ae. aegypti* Loqs-PA (left panels) and Loqs-PB (right panels) with the indicated probes corresponding to the DENV2 5' UTR, NS1, NS5 and 3' UTR sequences.

978 Top panel indicates a schematic representation of the position of the probes on the DENV genome
979 (not to scale). Probes were incubated with 2-fold dilutions of recombinant MBP-Loqs and
980 complexes were resolved on native polyacrylamide gels. The images of the free probe and the
981 Loqs-RNA complex for the 5' UTR are cropped from the same gel**. B.** Quantification of (A) with
982 dissociation constants for the indicated probes.

983 **Supplementary data legends**

984 **Figure S1. Expression of Loquacious isoforms in *Ae. aegypti* mosquitoes and depleted cells.**

985 **A.** Density plot of *Loqs* RNA seq reads in *Ae. aegypti*. Each line represents a unique sequence
986 library from three separate VectorBase datasets: DS_dcde6b4ec9, DS_24f2db6f66 and
987 DS_ded344cb5e [89–91]. **B-D.** Relative quantification of targeted gene mRNA expression from
988 Fig. 3E (S1B), 3F (S1C) and 3H-I (S1D). Gene expression was normalized to the housekeeping
989 gene *lysosomal aspartic protease* and expressed relative to expression in cells treated with control
990 dsRNA targeting luciferase (GL3, dashed horizontal lines). **E.** Total miRNAs at 48 h after infection
991 at a MOI of 0.1 in *Loqs*-depleted or control (GL3 luciferase dsRNA treated) Aag2 cells. Total
992 miRNA reads were normalized to tapiR1. **F.** Correlation of log2-transformed read per million
993 levels of known Ae. aegypti miRNAs in GL3 (x-axis) and Loqs (y-axis) dsRNA treated Aag2 cells
994 infected with DENV (left panel) or ZIKV (right panel). The sum of raw read counts of miRNAs
995 across three small RNA library replicates were calculated via Samtools. Highlighted are miRNAs
996 with > 2-fold differential expression with an adjusted p-value < 0.05 using DEseq2.

997

998

999 **Figure S2. Purification of recombinant Loqs-PA, -PB and interaction with dsRNA**

1000 **A.** Coomassie blue stained polyacrylamide gel containing lysates from the indicated purification
1001 steps of *Ae. aegypti* MBP-tagged Loqs-PA and Loqs-PB. **B.** Electrophoretic mobility assay of *Ae.*
1002 *aegypti* Loqs-PA (left panel) and Loqs-PB (right panel) with a 117 bp dsRNA corresponding to
1003 the firefly luciferase sequence. Probes were incubated with 5-fold dilutions of recombinant MBP-
1004 Loqs and complexes were resolved on native polyacrylamide gels. **C.** Quantification of (B) with
1005 dissociation constants for the indicated probes.

Figure S3. Uncropped gel images

A. Uncropped images of the western blots from Fig. 1A. **B.** Uncropped images of the EMSAs from Fig. 5A.

Figure S4. Uncropped IFA images

Uncropped images of IFAs from Fig. 4.

Table S1. Mass spectrometry hit summary

List of proteins enriched at least 2.5-fold in NS1 or NS5 immunoprecipitations with their -log10(*p*-value) and log2(fold change) values plotted on the volcano plot (Fig. 1D), the LFQ after row-mean subtraction plotted on the heatmap (Fig. 1E) as well as protein and gene identifiers in *Ae. albopictus* and references to orthologs in *Ae. aegypti*, *D. melanogaster* and *H. sapiens*. Individual values plotted on the heatmap were labeled when below (blue) or above (red) the row average. Proteins associated with both NS1 and NS5 are highlighted in yellow. Hits included in the STRING network (Fig. 2) and GO terms are indicated. Ost48 and Stt3A were included after literature review.

Table S2. GO term analysis data

Complete GO term analysis of Fig. 2A, including GO terms for cellular component (CC) and molecular function (MF).

Table S3. List of primers used for cloning, dsRNA production, qPCR, PCR and EMSA probes

Table S4. Reference sequences

List of protein sequences used as reference for sequence alignment illustrated in Fig. 4A.

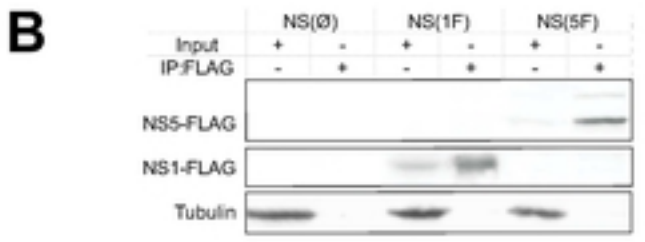

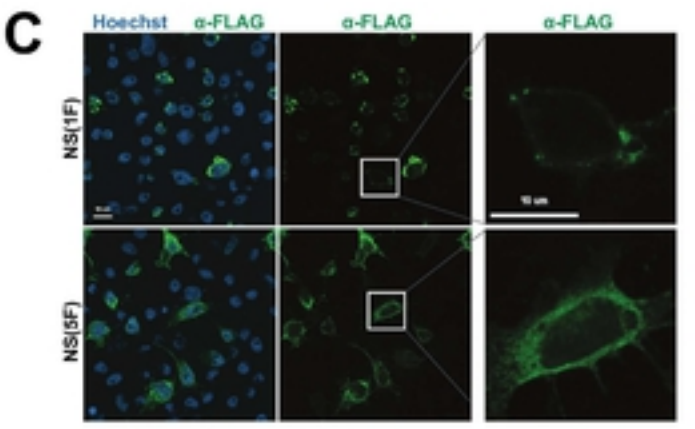

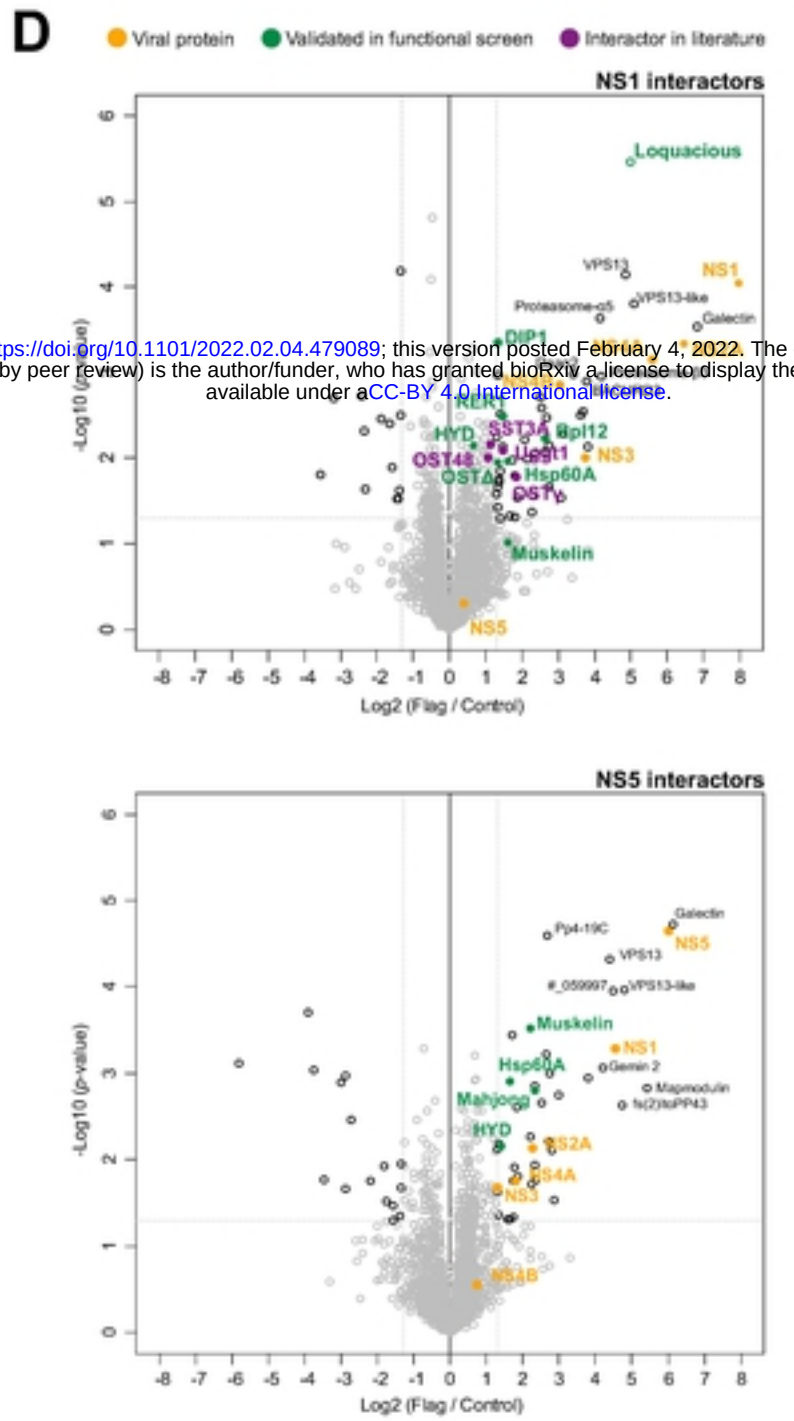

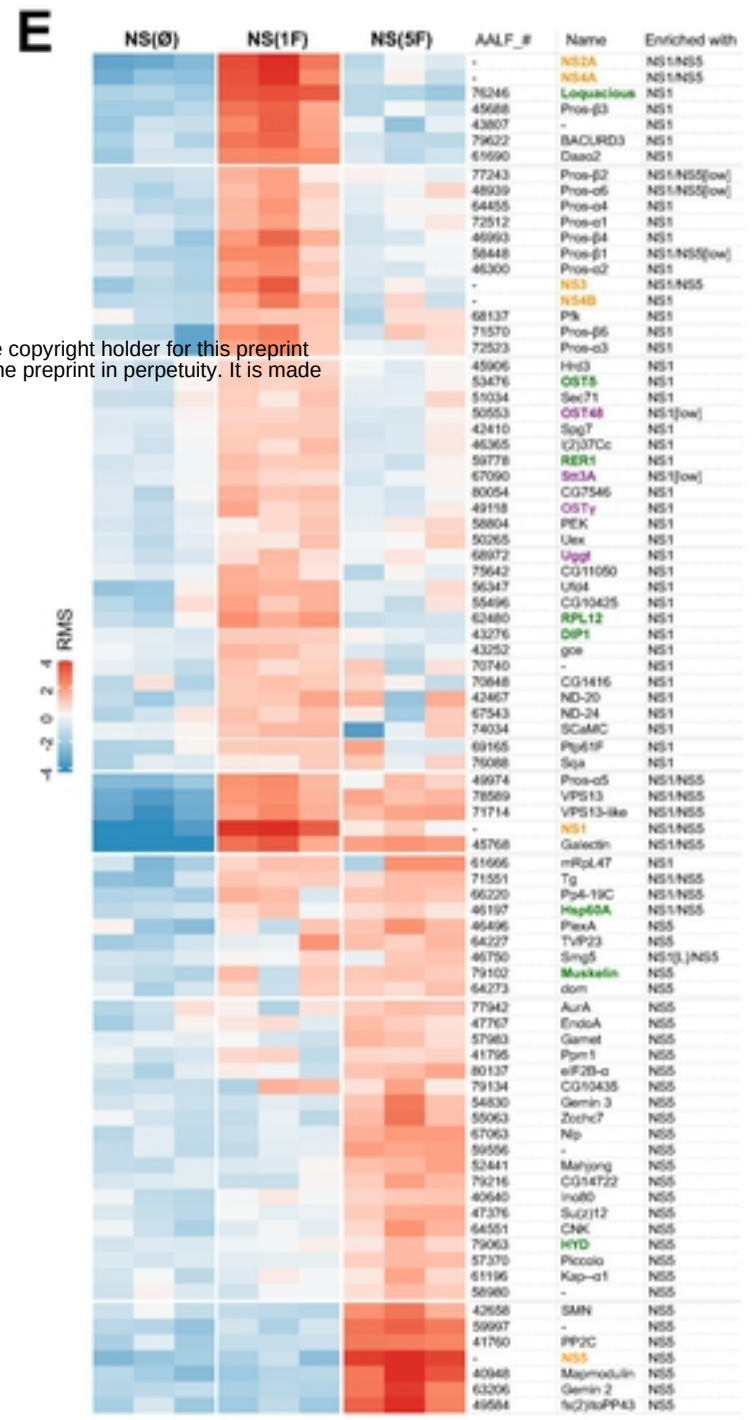

Fig. 1

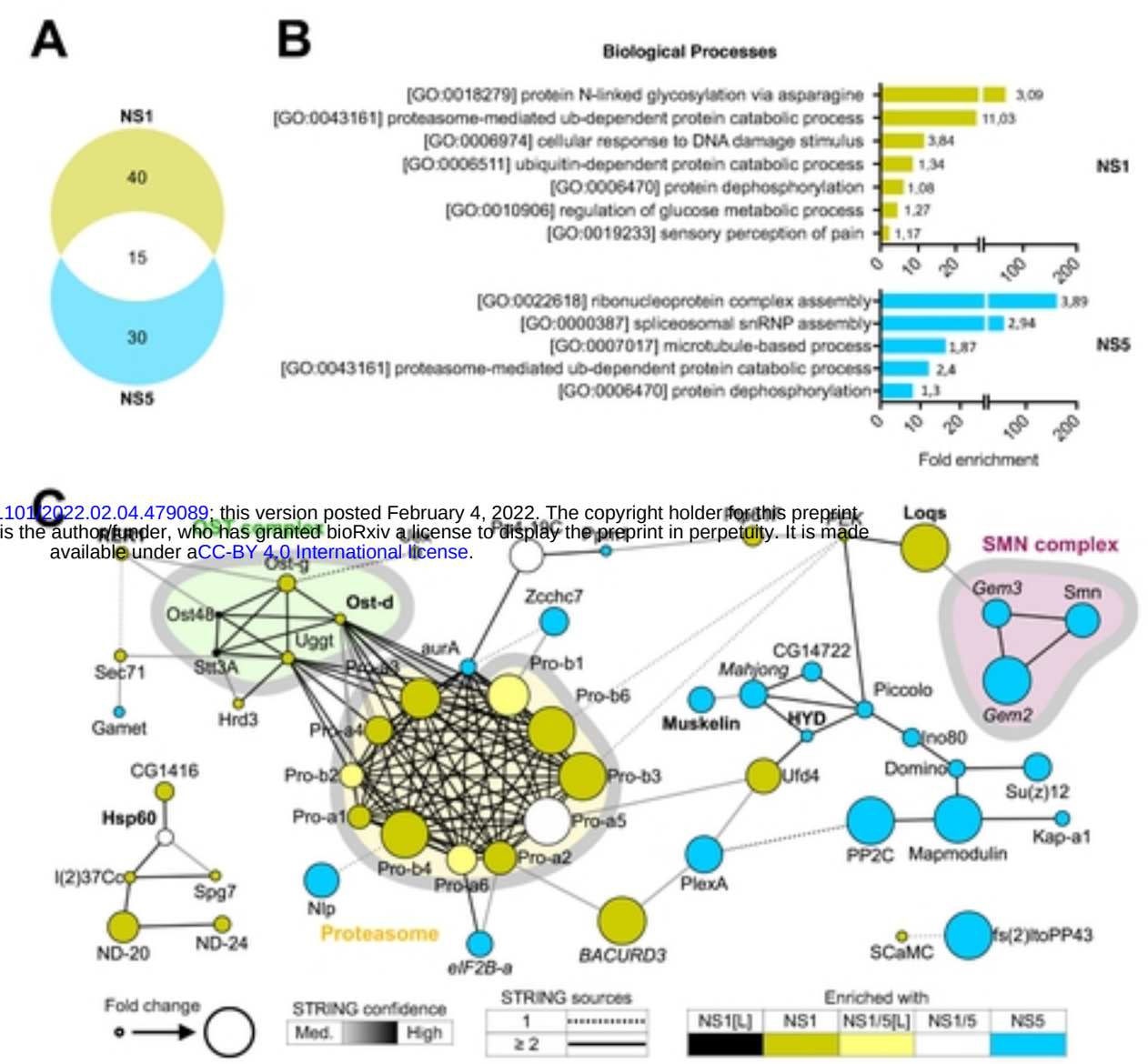

Fig. 2

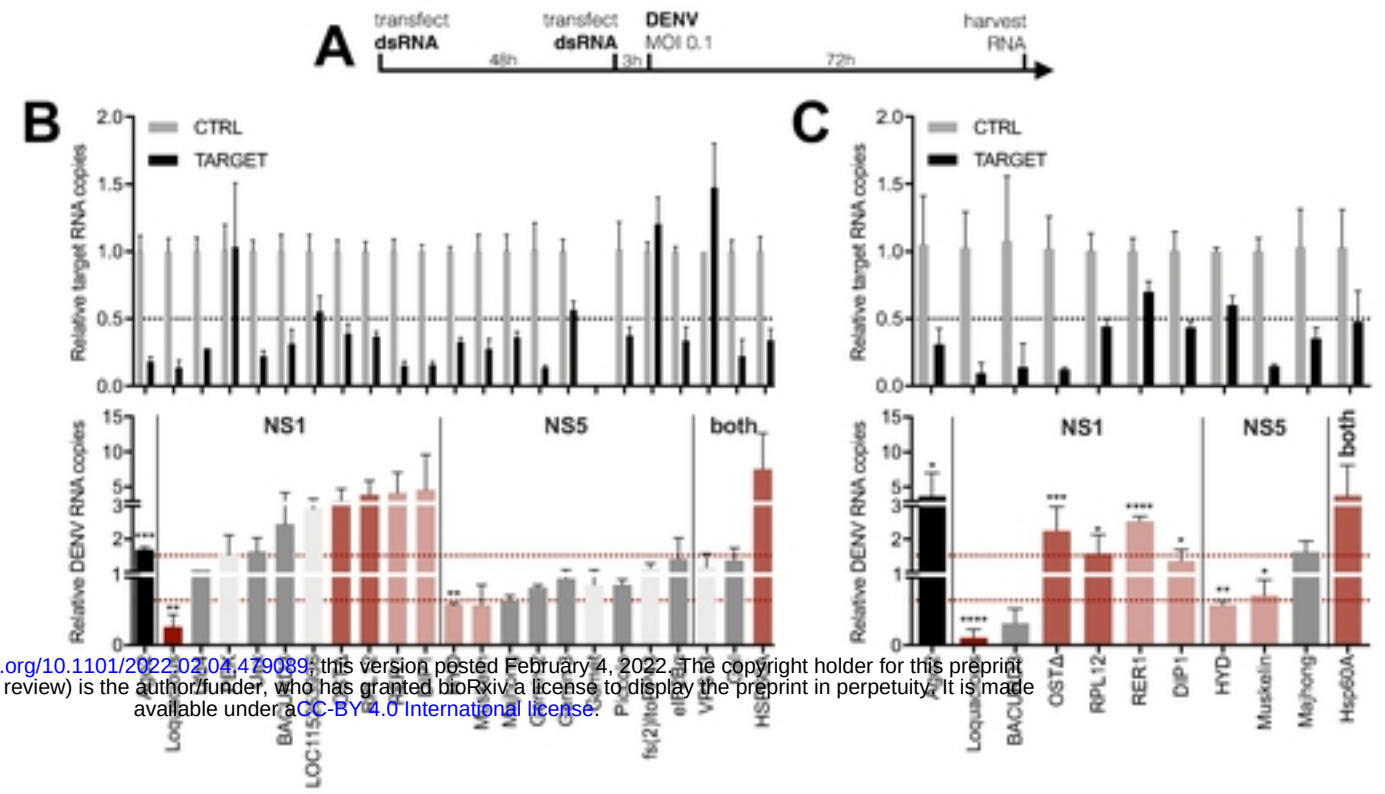

Fig. 3

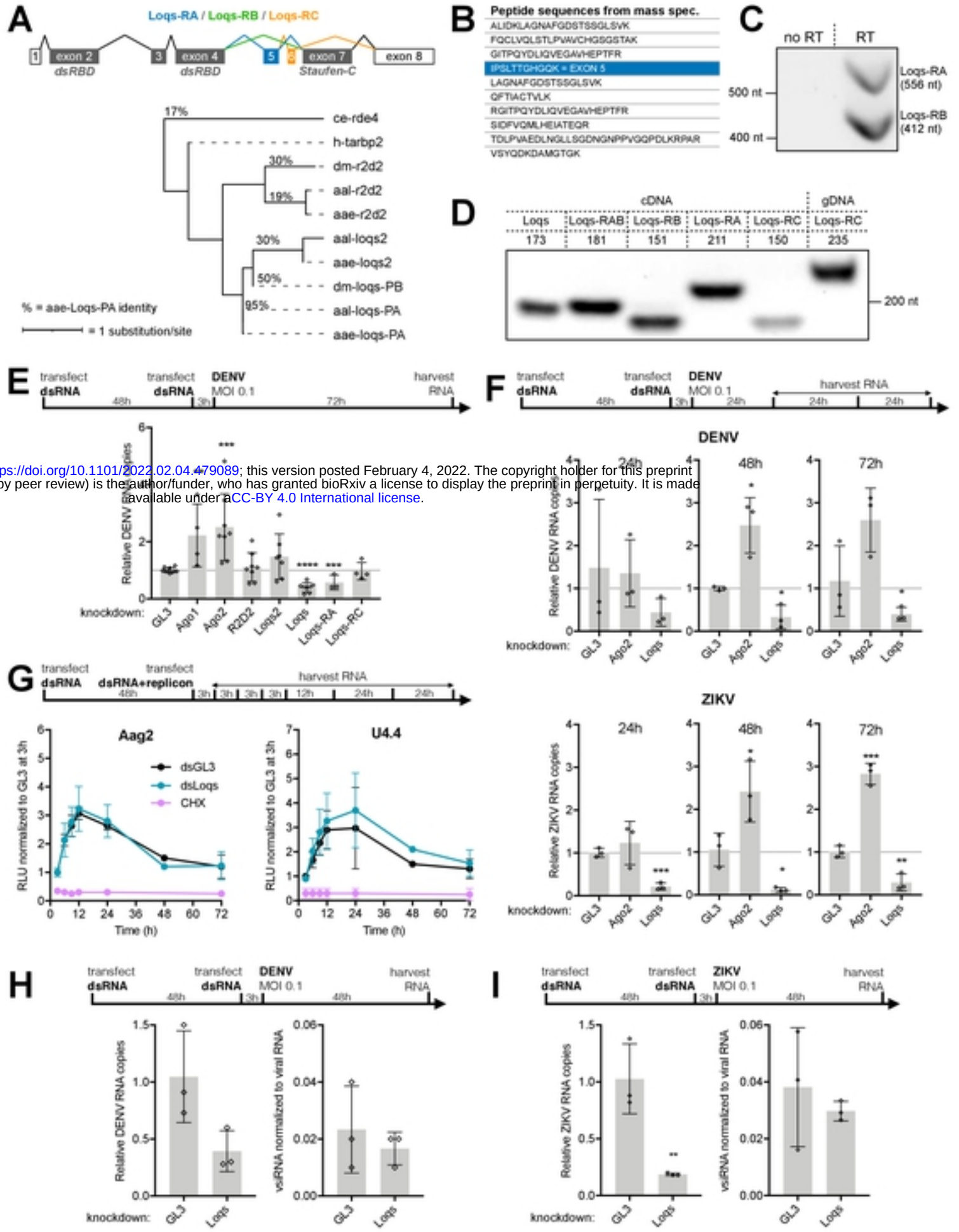

Fig. 4

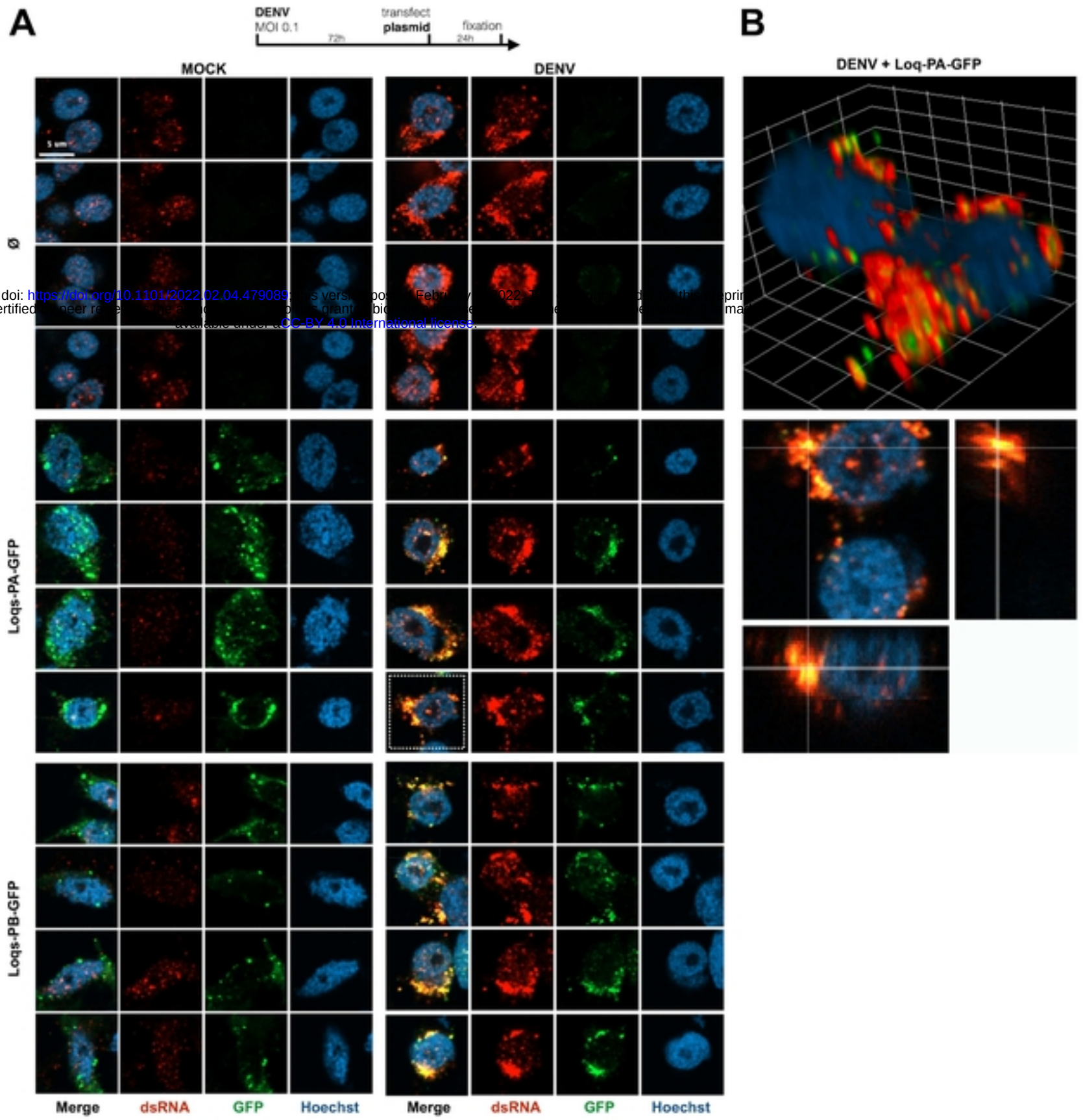

Fig. 5

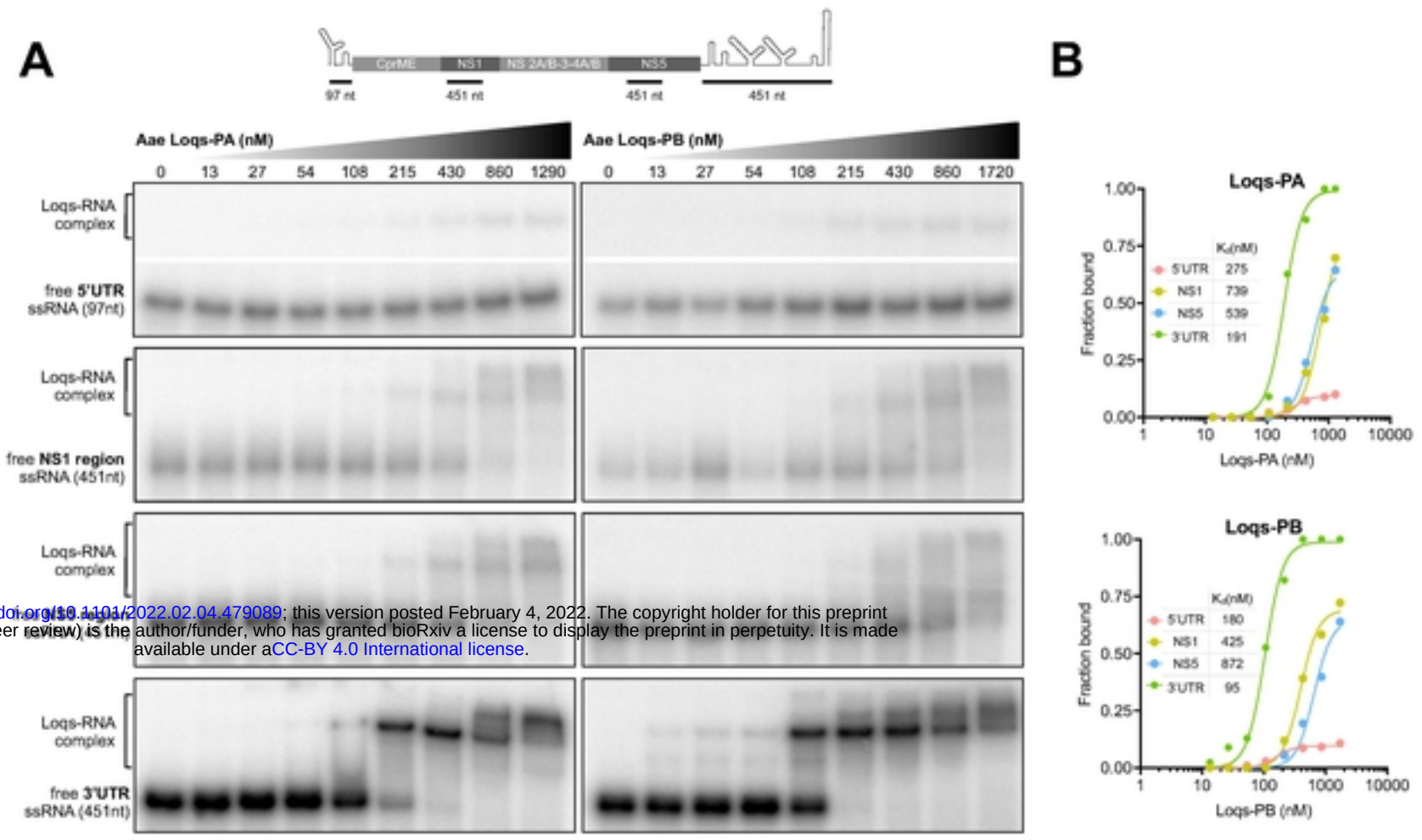

Fig. 6